PCCP

ROYAL SOCIETY OF CHEMISTRY

PAPER

View Article Online
View Journal | View Issue

Cite this: *Phys. Chem. Chem. Phys.*, 2025, **27**, 5739

A framework for designing main-group single-molecule magnets†

Akseli Mansikkamäki * and Anand Chekkottu Parambil

Single-molecule magnets (SMMs) are molecular entities with strongly anisotropic magnetic moment. As a result, SMMs display slow relaxation of magnetization at the macroscopic scale. Up to date all experimentally characterized SMMs are based on either d- or f-block metals with lanthanides proving to be the most successful. In the present work, a framework for constructing SMMs consisting purely of main-group elements will be outlined by computational and theoretical means. The proposed main-group SMMs utilize the strong spin–orbit coupling of a single heavy p-block atom or ion that can lead to strong magnetic anisotropy and pronounced SMM properties. A theoretical crystal-field model is developed to describe the magnetic properties of p-block SMMs with a minimal set of parameters related to the chemical structure of the SMMs. The model is used to establish which p-block elements and oxidation states can lead to SMM behavior. A large number of model structures are studied to establish general features of optimal chemical structures. These include one- and two-coordinate structures involving ligands with different coordination modes and all group 13 to 17 elements in periods 4 to 6. The results show that the most viable structures are based on mono-coordinated complexes of bismuth in oxidation state 0 with σ-donor ligands. Structures with bulkier ligands that sterically protect the bismuth atoms are then proposed as a starting point for the practical realization of main-group SMMs. The calculations show that minimizing the anagostic interactions with the bismuth atom is essential in the ligand design, which along with the low oxidation state of bismuth introduces significant synthetic challenges. The results do, however, show that main-group SMMs are plausible from a practical point of view within a limited set of heavier p-block elements in specific oxidation states. Furthermore, the proposed SMMs display much larger energy barriers for the relaxation of magnetization than even the best lanthanide-based SMMs do. This indicates that it is possible that main-group SMMs can supersede even the best currently known SMMs based on d- or f-block elements.

Received 19th December 2024,
Accepted 18th February 2025

DOI: 10.1039/d4cp04790g

rsc.li/pccp

1 Introduction

Single-molecule magnets (SMMs) are paramagnetic molecular entities, such as coordination complexes or endohedral metallofullerenes, that display slow relaxation of magnetization.[1–3] Slow relaxation is due to the bistable magnetic ground state with strong magnetic anisotropy at the molecular level. If an SMM is magnetized along a specific magnetic axis by an external field, it will remain in that direction for some time after the field is switched off. Therefore, the bulk crystal will remain magnetized until the magnetic states of the molecules relax to thermal equilibrium. Most mechanisms instigating the relaxation process are thermally activated,[2,4] and at sufficiently low temperature, referred to as the blocking temperature, the relaxation of magnetization is blocked within a given timescale. There is no universally agreed definition for the blocking temperature and its value depends on both the definition and the measurement conditions. During this period of relaxation the molecules retain information of the direction of the external field applied to it earlier and the magnetic state can be further modified by external perturbations. This means that SMMs can be used in quantum information processing. Grover's quantum algorithm has been implemented into an SMM in a proof-of-concept study,[5] and SMMs show potential in diverse applications in the fields of quantum computing and molecular spintronics.[6–12]

Although the first SMMs[1,2,13] were 3d transition metal systems, ever since the discovery of slow relaxation of magnetization in a terbium complex in 2003,[14,15] much of the focus in this field has switched towards lanthanide complexes.[3,16–20] All of the major advances in the blocking temperatures of SMMs over the past 15 years have been achieved with lanthanide

NMR Research Unit, University of Oulu, P.O. Box 8000, FI-90014, Finland.
E-mail: akseli.mansikkamaki@oulu.fi

† Electronic supplementary information (ESI) available: Detailed derivation of the theoretical model, additional computational data and optimized Cartesian coordinates. See DOI: https://doi.org/10.1039/d4cp04790g

systems, although there have been important advances also in the study of 3d and 5f systems.[21–24] Major advances in the case of lanthanide SMMs have been achieved by (i) modification of the crystal field (CF) around the lanthanide ion to produce a strongly axial CF with minimal equatorial contributions;[25–27] (ii) coupling two or more lanthanide ions into each other by using radical bridges;[28–31] and (iii) by mixed valence lanthanide compounds with covalent delocalized one-electron lanthanide–lanthanide bonds or quasi bonds.[32–35] Strategies (i) and (iii) have led to observation of magnetic hysteresis above the boiling point of liquid nitrogen.[25,33] The advances in strategy (i) are largely related to the detailed theoretical understanding of the interplay of the chemical structure, magnetic anisotropy and slow relaxation of magnetization.[18,36–40] This is due to the availability of high-accuracy quantum chemical *ab initio* methods[41–43] and the development of useful theoretical models.[36,44–46] In addition to understanding the effect of the static CF, much effort has been put in recent years to the understanding of the dynamic aspects of the magnetic properties through *ab initio* methods.[47–55] Strategy (i) has also been used to synthesize improved 3d metal-based SMMs.[56] A theoretical understanding of the design principles in strategy (ii) has been developed,[40,57–60] although they are not as well established as in the case of strategy (i). In the case of strategy (iii), some theoretical work has been published, but general design principles are still lacking.[32–34,61,62]

Currently design strategies (i) and (ii) are becoming rather mature, while design strategy (iii) is just emerging and its full potential has not yet been tested. Experience gained in all three strategies has shown that advancement in the study of SMMs requires an intimate understanding of the electronic structure of the type of system being studied to optimize their properties, as well as leaps into completely new types of systems and chemistries. Both aspects are important, perhaps even imperative, to take further strides forward in the field and to avoid stagnation which is always a risk that follows maturation. Therefore, it is important to actively consider completely new research directions that take the research outside the types of chemical structures actively studied and developed in design strategies (i)–(iii).

One possible new research direction – strategy (iv) – is to step out from the d and f blocks of the periodic table completely and to study the possibility of utilizing heavier main-group elements in the construction of SMMs. The completely different chemistry of these elements, compared to lanthanides, and their strong spin–orbit coupling (SOC)[63] are bound to lead to new kinds of properties if SMMs can be constructed from these elements. Furthermore, the advances made in the field of main-group chemistry over the past decade have made it possible to access an increasing number of p-block elements with low oxidation states and with low coordination numbers.[63–71] In a recent theoretical study we showed that the phenylbismuth anion could be utilized as the core moiety in an SMM consisting of purely main-group elements.[72] Furthermore, it was shown that the effective barrier for the reversal of magnetization could be almost four times as high as the highest barrier characterized in dysprosium-based SMMs. However, so far no SMM consisting purely of main-group elements has been experimentally characterized, and main-group elements have played only an auxiliary role in the study of SMMs.[73] Heavier main-group elements have been utilized as part of both diamagnetic and paramagnetic ligands,[74–78] but the principal origin of the magnetic anisotropy, that is necessary for the observation of slow relaxation of magnetization, has always been a d- or f-block element.

The purpose of the present work is to establish design strategy (iv); namely, a rigid foundation for the use of main-group elements as the main source of magnetic anisotropy in the construction of SMMs. The aim is to establish the design criteria both from a microscopic electronic structure point of view at the orbital level and from a point of view of the relevant chemical structures. The present work focuses on situations where the magnetic anisotropy originates from a single heavy p-block element atom or ion in a molecular structure. The framework is possible to extend in a rather straightforward way to situations where there is more than one such element in a molecular structure as long as the interaction between the heavy elements is weak; the extension follows the same logic as extending the theory of a monometallic lanthanide complex to a polymetallic lanthanide complex. Situations where there is a strong interaction between the heavy elements, such as a covalent bond, will be considered in future work.

This paper is organized as follows: in a short section following this Introduction, the terminology used in the paper is summarized. In Section 3 the design principles of main-group SMMs are discussed at a general qualitative level. In Section 4 a microscopic CF model is developed from first principles to understand which types of electronic configurations lead to slow relaxation of magnetization in main group systems, and how the different CF effects affect the magnetic properties. In Section 5 model chemical structures of main-group SMMs are studied by high-level quantum chemical methods. The results of the calculations along with the conclusions that can be made based on the model developed in Section 4 are used to establish the most viable route towards main-group SMMs. In Section 6 the results of Section 5 are then considered from a practical point of view by studying more realistic structures with appropriate steric protection, and several open challenges related to the practical synthetic realization of main-group SMMs are discussed. Finally, in Section 7 the main conclusions are summarized.

2 Note on terminology

We will use the terms 'main-group element', 'main-group atom' or simply 'metal' to refer to the central atom or ion in a compound that will contribute the unpaired electrons to the system. The rest of the molecule will be referred to as ligands. The metal–ligand bond in the structures considered in the present work is best described as a coordination bond with the main-group element acting as a Lewis acid and the ligands

acting as Lewis-basic electron donors. Thus, we will use the terminology of coordination chemistry and discuss all bonds between the ligands and the main-group element as coordination bonds with the ligands acting as electron donors, although in the case of some of the more electronegative main-group elements considered, this description is not ideal. Of all the elements considered in this work, bromine and iodine are more electronegative than the ligand donor atoms (carbon and nitrogen),[79] and in this case the assignment of oxidation states by assuming that the electron pair of the metal–ligand bond belongs to the ligand is not logical considering the usual rules for assigning oxidation states, but such an assignment will be used to keep the discussion between all the elements consistent. It should be emphasized that we will not consider the formation or dissociation of bonds between the main-group element and the ligands. Thus, the origin or fate of the bonding electrons, *i.e.*, whether they originated from a metal, ligand or both, or where they end up upon dissociation is irrelevant in practice.

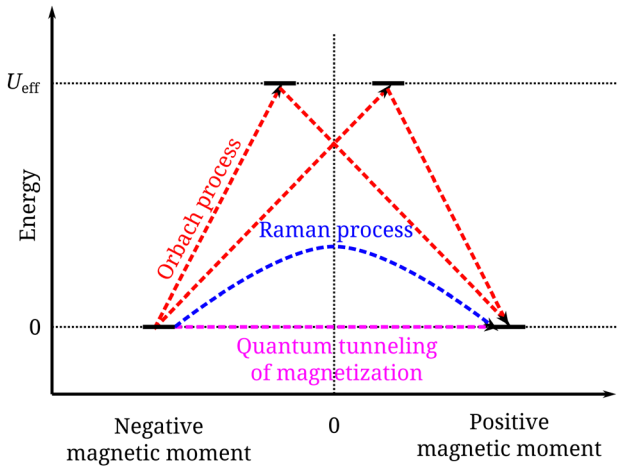

Fig. 1 A schematic representation of the different mechanisms that mediate transitions between different electronic states of an SMM. The transitions instigate relaxation of the magnetization by reorientation of the molecular magnetic moment from a negative direction to a positive direction along the main magnetic axis.

3 General design principles

3.1 Electronic structure of single-molecule magnets

The ground-state of an SMM consists of two magnetic states corresponding to different orientations of the magnetic moment. A further requirement is that direct electronic transitions between these states are improbable enough leading to the observations of the slow magnetization dynamics at the macroscopic level. In the case of Kramers systems (*i.e.*, systems with odd number of electrons), the ground state is exactly two-fold degenerate due to Kramers' theorem[80,81] and constitutes a Kramers doublet (KD). In the case of non-Kramers systems (*i.e.*, systems with even number of electrons), the ground doublet can be a quasi doublet which is almost degenerate or an Ising doublet which is exactly degenerate due to some point-group symmetry of the molecule.[39,82] There are two mechanisms for the reorientation of the molecular magnetic moment: spin–phonon coupling and quantum tunneling of magnetization (QTM, Fig. 1). The former originates from the interaction of the magnetic state of the molecule with the vibrations of the crystal lattice, *i.e.*, the phonons, and the latter originates from the mixing of the two states in the ground doublet under the CF (only in non-Kramers systems) or due to magnetic fields originating from nuclear spin or neighboring molecules (in both Kramers and non-Kramers systems).[2,4,83] Spin–phonon relaxation is dominant in high temperature and QTM in low temperature.

Spin–phonon relaxation can take place either by direct transitions between the two components of a doublet or through an intermediate state belonging to an excited doublet. Direct transitions are forbidden in a situation where the ground doublet is exactly degenerate.[83] Thus, no spin–phonon transitions take place between the two states of a KD unless there is a strong external magnetic field that splits the doublet.[84] This means that one-phonon spin–phonon relaxation in a Kramers system requires transitions by at least one excited state. This is known as the Orbach process (Fig. 1). Its rate is proportional to an exponential factor $\exp(-U_{eff}/k_BT)$ similar to the Arrhenius equation of reaction rates.[85] The exponential factor depends on the effective barrier height U_{eff}, temperature T and Boltzmann constant k_B. The barrier height U_{eff} is the energy difference between the ground state and the highest electronic state involved in the process; thus, it is directly related to the static electronic structure of the system. In the first- and second-order Raman processes the electronic system interacts with a superposition of phonons. The rate is independent of the energy difference and can take place between the two components of a KD. The Raman process has a power-law dependence of the temperature with various possible exponents.[86]

If we assume that the Orbach process is the dominant spin–phonon relaxation mechanism, SMMs can be improved by (i) increasing the effective barrier height U_{eff} and (ii) blocking the QTM in the ground KD. Blocking of the QTM is related to the axiality[46,87] of the KD which is directly related to the magnetic anisotropy of the system. The magnetic axiality of a KD is usually described in terms of a pseudospin Zeeman Hamiltonian:[41,83,88–91]

$$\tilde{H} = \mu_B \mathbf{B}\cdot\mathbf{g}\cdot\tilde{\mathbf{S}}, \quad (1)$$

where μ_B is the Bohr magneton, $\mathbf{B}$ is the external magnetic field, $\mathbf{g}$ is the pseudospin $\mathbf{g}$ tensor and $\tilde{\mathbf{S}}$ is the pseudospin operator that acts on the two-dimensional space spanned by the components of the KD. By a proper choice of coordinate axes, the pseudospin $\mathbf{g}$ tensor can always be brought to a diagonal form with three principal components g_X, g_Y and g_Z corresponding to a set of principal magnetic axes.[92] In the case of isotropic systems the principal components are all equal $g_X = g_Y = g_Z$, whereas in axial anisotropy $g_Z > g_X,g_Y$, and in non-axial anisotropy $g_Z < g_X,g_Y$. The Z axis is chosen as the principal magnetic axis by convention, whereas the X and Y components

are referred to as the transverse components. In an ideally axial system $g_X = g_Y = 0$ and $g_Z \neq 0$. In such a situation only the component of the magnetic field along the principal magnetic axis, *i.e.*, the Z axis, contributes to the Zeeman splitting creating a very strong axial magnetic anisotropy. Relaxation by QTM is proportional to the transverse components g_X and g_Y, and in an ideally axial KD, QTM is suppressed.[2,39,87]

In the present work, we will mostly focus on two aspects in the design of SMMs: the axiality of the ground doublet and the magnitude of the effective barrier height U_{eff}. Both of these are static properties of the system and they can be studied without considering the dynamic interactions of the systems with the phonons. Axial ground doublet and high U_{eff} are necessary preconditions for SMMs with a high blocking temperature, but ultimately the blocking temperature is determined by the dynamic properties. The efficiency of the Raman process cannot be associated with any single feature of the static electronic structure. Furthermore, it is possible that the temperature-dependence of the relaxation rate does not follow the well-established laws.[47,54,55,93] Significant advances in understanding more complex features of the relaxation process have been made over the past years,[48–52,94] but a detailed study of the dynamic aspects related to main-group SMMs is well beyond the scope of the present work but will be considered in the future.

3.2 Geometries of main-group single-molecule magnets

The valence p orbitals of main-group elements have large spatial extents and they actively take part in the formation of covalent chemical bonds. In terms of CF theory, this corresponds to the strong-field case,[83,95,96] where the splitting of one-particle functions, *i.e.*, atomic orbitals, under the effect of the CF are considered first, and the electronic configurations are then constructed within this split orbital set following the *aufbau* principle. Electron–electron repulsion and SOC are introduced in subsequent steps to yield the electronic states. In the case of main-group elements only the valence p shells contribute to the total orbital momentum at first order, since s shells have zero orbital momentum. Therefore, we focus explicitly on the valence p orbitals, labeled as np where n is the principal quantum number. The role of s orbitals in the bond formation of heavier main group elements is in any case greatly reduced by the inert-pair effect and can be neglected to a first approximation.[97–99]

Magnetic anisotropy originates from anisotropic orbital angular momentum that is coupled by SOC to the spin to yield an anisotropic magnetic moment. Typically SOC in the context of main-group elements is considered as a second-order perturbation due to the lack of orbital degeneracies as is the case in the famous El-Sayed rules in optical spectroscopy.[100,101] However, a necessary precondition for strong magnetic anisotropy is a partially unquenched orbital momentum and unpaired electrons which lead to a nonzero spin. Ideal axial orbital momentum requires that the X and Y components of the orbital momentum are quenched whereas the Z component is nonzero. Due to the Kramers' theorem nonzero one-electron orbital momentum is only possible if at least two of the np orbitals are degenerate.[83] If all three np orbitals were degenerate, they would form an irreducible spherical set, and the orbital angular momentum would be isotropic. Thus, two of the orbitals must be degenerate while one of them lies sufficiently lower or higher in energy. It is trivial to show by calculations that in order to have a non-zero angular momentum along the Z axis, the two degenerate orbitals must be the $n\text{p}_x$ and $n\text{p}_y$ orbitals. In practice, near degeneracy of the $n\text{p}_x$ and $n\text{p}_y$ orbitals is sufficient.

A situation where the $n\text{p}_x$ and $n\text{p}_y$ orbitals are degenerate and the $n\text{p}_z$ orbital is energetically removed from these orbitals will arise when (i) the $n\text{p}_x$ and $n\text{p}_y$ orbitals are strictly non-bonding and their energy is not biased by any electrostatic interaction; or (ii) the $n\text{p}_x$ and $n\text{p}_y$ orbitals form a basis for a two-dimensional degenerate irreducible representation of the molecular point group; or both (i) and (ii). Conditions (i) and (ii) are simultaneously fulfilled in a one- or two-coordinate system with linear geometry and strictly σ-donating ligands. The respective qualitative molecular orbital diagrams are shown in Fig. 2a and b. In realistic systems an ideal $C_{\infty\text{v}}$ or $D_{\infty\text{h}}$-symmetric geometry is not possible, as a strictly linear system would be unstable. The axial $C_{\infty\text{v}}$ and $D_{\infty\text{h}}$ point groups are also incompatible with any crystal symmetry and cannot be realized in the solid state. The lower symmetry beyond the first coordination sphere will lead to some splitting between the π-symmetric $n\text{p}_x$ and $n\text{p}_y$ orbitals, but if π-type bonding is minimal the splitting should be weak, and condition (i) is approximately fulfilled.

Condition (ii) but not (i) is realized in systems where the $n\text{p}_x$ and $n\text{p}_y$ orbitals take part in bonding but which have a sufficiently high symmetry so that the $n\text{p}_x$ and $n\text{p}_y$ orbitals form a basis for degenerate irreducible representations of the point group. These groups include all point groups with a threefold or higher proper or improper rotational axis: C_x, $C_{x\text{v}}$, $C_{x\text{h}}$, D_x, $D_{x\text{h}}$, $D_{x\text{d}}$ and S_x with $x \geq 3$, as well as the group $D_{2\text{d}}$. In the cubic and icosahedral groups T, T_h, T_d, O, O_h, I and I_h all three np orbitals are equivalent which means that there would be no splitting between the $n\text{p}_x$, $n\text{p}_y$ and $n\text{p}_z$ orbitals and they are unsuitable for main-group SMMs. A qualitative molecular orbital diagram for the bonding in a trigonal-planar $D_{3\text{h}}$ symmetric system is shown in Fig. 2c. More complicated bonding situations will lead to a similar molecular-orbital diagram, but introduction of axial ligands (for example, trigonal-bipyramidal geometry with $D_{3\text{h}}$ symmetry) might change the energetic ordering of the $n\text{p}_x$, $n\text{p}_y$ and $n\text{p}_z$ orbital sets.

The situation where both conditions (i) and (ii) are realized is more ideal because the involvement of the $n\text{p}_x$ and $n\text{p}_y$ orbitals in bonding leads to the reduction of the strength of the SOC due to the relativistic nephelauxetic effect.[102,103] This will weaken the anisotropy. However, a much more severe problem that arises when (ii) is realized and (i) is not, is the distortion of the structure towards lower symmetry that will break orbital degeneracy due to the Jahn–Teller effect[104,105] as shown in Fig. 3. In principle, the strong SOC of the heavier

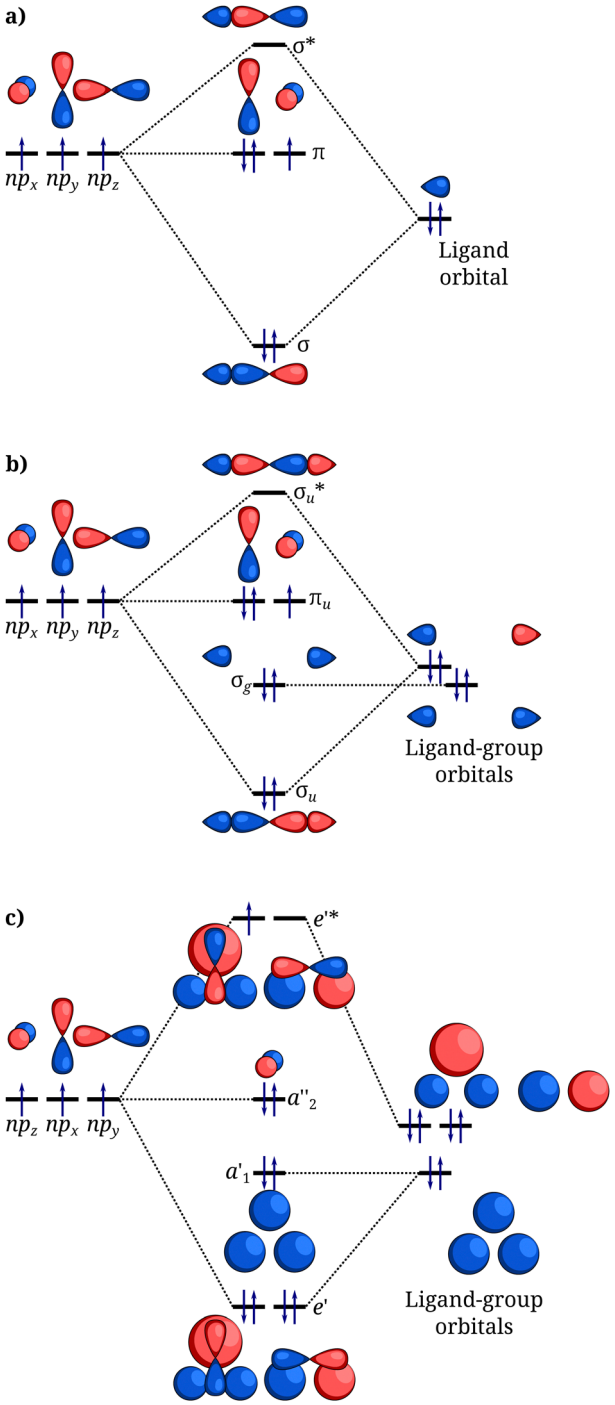

Fig. 2 Qualitative molecular orbital diagrams describing the bonding between the *n*p orbitals of a heavy main group element and ligand orbitals in case of (a) a single purely σ-donating ligand ($C_{\infty v}$ symmetry); (b) two purely σ-donating ligands in a linear geometry ($D_{\infty h}$ symmetry); (c) three pure σ-donating ligands in a trigonal-planar geometry (D_{3h} symmetry). The electrons in the diagrams are drawn to correspond to a group 15 element with three valence *n*p electrons.

p-block elements can quench the Jahn–Teller effect and stabilize a symmetric geometry with orbital degeneracy. This has been shown to be the case in some d-block complexes.[106,107] However, due to the large spatial extent of the *n*p orbitals, they

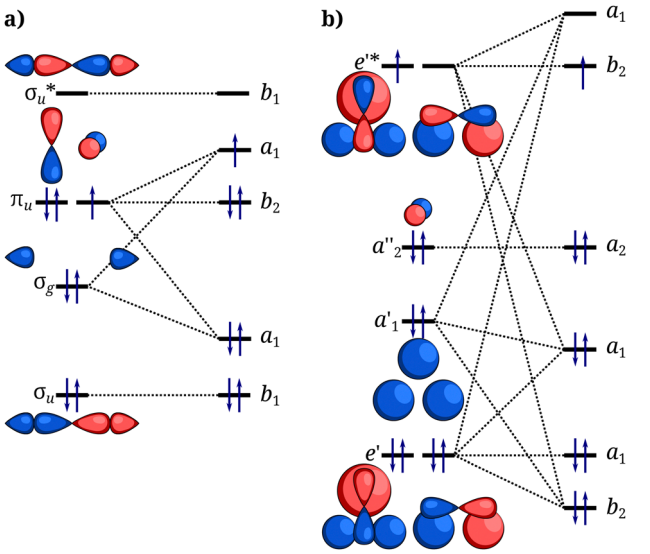

Fig. 3 Qualitative molecular orbital diagrams describing the splitting of orbitals under a C_{2v} distortion of (a) a two-coordinate $D_{\infty h}$-symmetric structure described in Fig. 2b; and (b) a three-coordinate D_{3h}-symmetric structure described in Fig. 2c.

tend to have large overlaps between the ligand orbitals and are especially prone to Jahn–Teller distortions. For example, these distortions are one of the main reasons for the lone-pair effect that makes multiple bonding between heavier main-group elements increasingly unlikely.[108,109] The distortions are minimized if the overlap between the np_x and np_y orbitals and the ligand orbitals is minimized – condition (i) – or in the case when the main group element is mono-coordinated and there is no local distortion that could lift the degeneracies such as shown in Fig. 2a. Based on these arguments, the conditions for the ideal geometries can be revised as follows: condition (i) is retained and condition (ii) is important but only when it is subject to condition (i).

These conditions limit the geometries essentially to one- and two-coordinate linear systems with purely σ-donating ligands and no π-type metal–ligand interaction. In principle, the conditions also allow higher coordination numbers as long as the two np_x and np_y orbitals are degenerate by symmetry and do not participate in the metal–ligand bonding. However, due to the large spatial extent of the *n*p orbitals and their strong tendency to form covalent bonds, it is very unlikely that if ligands were introduced into equatorial coordination positions that the np_x and np_y orbitals would not display any covalency with the ligands. Thus, the one- and two-coordinate geometries where only the np_z orbital forms covalent bonds are a much more promising approach.

3.3 Electronic configuration of main-group single-molecule magnets

The np_z orbital forms a one bonding combination with a ligand donor orbital and one anti-bonding combination. The bonding combination is occupied by two ligand electrons. The non-bonding degenerate np_x and np_y orbitals lie between the

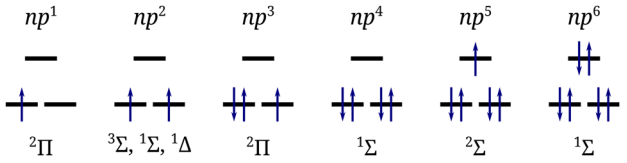

Fig. 4 The *aufbau* electronic configurations (second row) that arise from a given free atom or ion valence *n*p configuration (top row) and the possible terms that arise from the *aufbau* configuration under ideal axial symmetry (bottom row).

bonding and anti-bonding np_z orbital combinations. Thus, the electrons from the *n*p shell start first occupying the np_x and np_y orbitals and then the anti-bonding np_z orbital as shown in Fig. 4. This is also consistent with an electrostatic CF picture where the np_z orbital is increased in energy due to the electrostatic repulsion between the orbital and the ligand donor electron pairs. Since the interaction of the np_z orbital with the ligand is covalent, the splitting between the np_x, np_y set and the anti-bonding np_z is large, and the orbitals are filled following the *aufbau* principle. This is equivalent to the strong CF limit where high-spin configurations are not possible, and for each number of *n*p electrons, there is only one possible electron configuration.

While the electrons occupying the np_x, np_y set have axial anisotropic one-electron orbital angular momentum, the angular momenta need to be coupled in the many-electron state in such a way that also the many-electron state has anisotropic orbital angular momentum. In an ideal axial geometry, before the inclusion of SOC, the electronic states are eigenstates of the total spin operators $\hat{S}^2$ and $\hat{S}_z$ as well as the total orbital angular momentum projection $\hat{L}_z$. The states arising from a given *aufbau* configuration can then be characterized by the total spin multiplicity $2S + 1$ and the angular momentum projection M_L in terms $^{2S+1}M_L$ such as in the case of the electronic states of diatomic molecules.[110] The electronic states arising from a given configuration are shown in Fig. 4. Orbital momentum is quenched in the Σ states and configurations that only give rise to Σ terms cannot lead to SMM behavior. The spin doublet terms arising from the np^1 and np^3 configurations have a nonzero orbital momentum. The configuration np^2 gives rise to three terms: a spin triplet with no orbital momentum $^3\Sigma$, a spin singlet with no orbital momentum $^1\Sigma$ and a spin-singlet with nonzero orbital momentum $^1\Delta$. Based on Hund's rules the ground term is the spin triplet $^3\Sigma$. However, this term can mix with the excited $^1\Delta$ term under SOC. This means that the $^3\Sigma$ term can split under SOC in second order to yield anisotropic states albeit the anisotropy should be weaker than in the case of the np^1 and np^3 states where it arises at the zeroth order. If the CF splitting was weak, high-spin configurations with unquenched orbital momentum would also be possible in the case of the np^4 configuration. However, in all systems considered in the present work, the CF splitting is too strong to stabilize a high-spin configuration.

Based on these considerations, the possible main-group SMMs can be limited to one- or two-coordinate linear, or close to linear systems where the np_x and np_y orbitals retain their atomic character and do not take part in bonding in a significant manner. Furthermore, the number of valence *n*p electrons should be either one, two or three.

4 Theoretical model

4.1 General model features

The purpose of the theoretical model is to explain the anisotropic magnetic properties of a main-group SMM with minimal complexity and a minimal number of parameters. Furthermore, the parameters should have a chemical interpretation. Only the main results are given here and a full derivation of the results is given in the ESI.† The results are derived explicitly in the np^1, np^2 and np^3 cases which are relevant for the design of main-group SMMs as discussed in Section 3.

The starting point of the model is the two degenerate or near-degenerate p orbitals chosen as the real np_x and np_y orbitals. The np_z orbital takes part in the formation of a coordination bond, and is energetically sufficiently well removed from the np_x and np_y orbitals, that it does not need to be considered in the model. In the strong-field case of p-block elements, this can be assumed. The model is constructed in accordance with CF theory that only considers pure atomic-like np_x and np_y orbitals. It is assumed that the role of these orbitals in metal–ligand covalency is minimal. The covalency and electrostatic interaction with the ligand is implicitly taken into account by a one-electron CF potential operator $\hat{V}_{\mathrm{CF}}$. The one-electron nature of the operator introduces another approximation. The effect of the CF is reduced into two parameters: the diagonal CF parameter Δ which describes the splitting between the np_x and np_y orbitals and the off-diagonal CF parameter η which describes the mixing between np_x and np_y in the lower symmetry of the molecule.

To simplify the mathematical treatment, the CF Hamiltonian $\hat{H}$ is constructed on the basis of the complex p orbitals np_{-1} and np_{+1}:

$$|np_{\pm 1}\rangle = \mp\frac{1}{\sqrt{2}}\left(|np_x\rangle \pm i|np_y\rangle\right). \tag{2}$$

The CF Hamiltonian is written in a second-quantized form as

$$\begin{aligned}\hat{H} = &\sum_{m_l,m_l'}\sum_{m_s,m_s'}\left\langle n,l,m_l,s,m_s\middle|\hat{h}+\hat{V}_{\mathrm{CF}}+\hat{\xi}\hat{\mathbf{s}}\cdot\hat{\mathbf{l}}\middle|n,lm_l',sm_s'\right\rangle\hat{a}^{\dagger}_{m_lm_s}\hat{a}_{m_l'm_s'}\\ &+\sum_{\substack{m_l,m_l'\\ m_l'',m_l'''}}\sum_{m_s,m_s'}\left(n,lm_l;n,lm_l'\middle|n,lm_l'';n,lm_l'''\right)\\ &\times\hat{a}^{\dagger}_{m_l,m_s}\hat{a}^{\dagger}_{m_l'',m_s'}\hat{a}_{m_l''',m_s'}\hat{a}_{m_l',m_s},\end{aligned} \tag{3}$$

where $\hat{a}^{\dagger}_{m_l,m_s}$ and $\hat{a}_{m_l,m_s}$ are electron creation and annihilation operators, respectively, $\hat{h}$ is the spherically symmetric part of the one-electron operator, which includes the kinetic energy operator, correction terms for scalar relativistic effects and the electron–nucleus attraction between the central main-group

atom or ion, $\hat{\xi}$ is the radial part of the one-electron SOC operator, and $\hat{\mathbf{l}}$ and $\hat{\mathbf{s}}$ are the one-particle orbital and spin angular momentum operators, respectively. $(n, lm_l; n, lm_l' | n, lm_l''; n, lm_l''')$ are electron–electron repulsion integrals given in the chemist's notation.[111] The one-particle basis states are labeled by the principal quantum number n, the orbital and spin angular momentum quantum numbers l and s, respectively, and the projections of the orbital and spin angular momentum on the quantization axes m_l and m_s, respectively. In all cases considered $s = 1/2$ and $l = 1$, and the labels l and s are dropped on the creation and annihilation operators. As is common in CF treatments, the two-particle SOC and spin–spin coupling terms are neglected.

Within the chosen basis of the $n\mathrm{p}_x$ and $n\mathrm{p}_y$ orbitals the structure of the Hamiltonian (3) simplifies considerably. Furthermore, since we are only interested in the energy differences between different states that arise from a given $n\mathrm{p}^N$ configuration, we can remove all terms that contribute equally to the different states by translation of the energy origin. The simplified form of the Hamiltonian reads

$$\hat{H} = \sum_{m_s}\left(\gamma \hat{a}^\dagger_{-1,m_s}\hat{a}_{+1,m_s} + \gamma^* \hat{a}^\dagger_{+1,m_s}\hat{a}_{-1,m_s}\right) + \zeta \sum_{m_l}\sum_{m_s} m_l m_s \hat{n}_{m_l,m_s} - \frac{K}{2}\sum_{m_l}\sum_{m_s,m_s'} \hat{a}^\dagger_{m_l,m_s}\hat{a}^\dagger_{-m_l,m_s'}\hat{a}_{-m_l,m_s}\hat{a}_{m_l,m_s'}, \quad (4)$$

where $\hat{n}_{m_l,m_s} = \hat{a}^\dagger_{m_l,m_s}\hat{a}_{m_l,m_s}$ is a number operator. The parameters of the Hamiltonian are the complex CF parameter γ that is related to the CF parameters of the real orbitals as

$$\gamma = -\frac{1}{2}\Delta - i\eta, \quad (5)$$

the real one-electron SOC integral ζ, that is usually a positive number,[112] and the real positive two-electron exchange integral $K = (n, lm_l; n, lm_l' | n, lm_l'; n, lm_l)$ where $l = 1$ and $m_l = -m_l'$. If the exchange integral K is transformed to a real-orbital basis, it will constitute a contribution from both a Coulomb integral and an exchange integral but in a complex spherical basis these are reduced to a single parameter.

4.2 Symmetry considerations

A total of four different real parameters are needed to define the model. In the case of high molecular point-group symmetry, the number of CF parameters can be reduced to zero, so that only K and ζ are needed. The real CF parameters Δ and η, and consequently the complex parameter γ, vanish in point-group symmetries where the $n\mathrm{p}_x$ and $n\mathrm{p}_y$ orbitals are equivalent; *i.e.*, they form a basis for a two-dimensional irreducible representation of the group. These groups include all molecular point groups with a threefold or higher proper or improper rotational axis: C_x, C_{xv}, C_{xh}, D_x, D_{xh}, D_{xd} and S_x with $x \geq 3$, as well as the group D_{2d}. These groups will lead to an ideal axial CF.[46,87] In the cubic and icosahedral groups T, T_h, T_d, O, O_h, I and I_h all three np orbitals are equivalent leading to spherical symmetry of the orbital momentum. Thus, these groups have too high a symmetry for observing SMM behavior. In groups where the $n\mathrm{p}_x$ and $n\mathrm{p}_y$ orbitals transform according to different irreducible representations of the point group, the parameter η vanishes but Δ can have a non-zero value. These groups include C_s, C_{2v}, D_2 and D_{2h}. In the case when $\eta = 0$ but $\Delta \neq 0$, the complex CF parameter γ becomes real.

It is worth noting that the requirements for the disappearance of the CF splitting and mixing of the orbitals in the case of p-block SMMs are lower than in the case of d- or f-block SMMs. In the case of d-orbitals a fivefold proper or improper axis is required and in the case of f-orbitals a sevenfold axis is needed.[3,39,87]

4.3 $n\mathrm{p}^1$ case

In the simplest case of one electron, the basis states can be constructed by creating an electron on the orbital m_l with spin projection m_s on an otherwise empty orbital space:

$$\hat{a}^\dagger_{-1,-1/2}|n\mathrm{p}^0\rangle,\ \hat{a}^\dagger_{+1,-1/2}|n\mathrm{p}^0\rangle,\ \hat{a}^\dagger_{-1,+1/2}|n\mathrm{p}^0\rangle \text{ and } \hat{a}^\dagger_{+1,+1/2}|n\mathrm{p}^0\rangle. \quad (6)$$

Within this basis the Hamiltonian is

$$H^{1\text{-elec}} = \begin{pmatrix} \zeta/2 & \gamma & 0 & 0 \\ \gamma^* & -\zeta/2 & 0 & 0 \\ 0 & 0 & \zeta/2 & \gamma^* \\ 0 & 0 & \gamma & -\zeta/2 \end{pmatrix} \quad (7)$$

and has two doubly degenerate eigenvalues

$$E^{1\text{-elec}}_{\pm} = \pm\sqrt{\frac{\zeta^2}{4} + |\gamma|^2} = \pm\frac{1}{2}\sqrt{\zeta^2 + \Delta^2 + 4\eta^2}. \quad (8)$$

Thus, the energy level structure consists of two KDs. If the system displays Orbach-type relaxation, the effective barrier would be the energy difference between the KDs:

$$U_{\mathrm{eff}} = E^{1\text{-elec}}_{+} - E^{1\text{-elec}}_{-} = \sqrt{\zeta^2 + \Delta^2 + 4\eta^2}. \quad (9)$$

The $\mathbf{g}$ tensor of the ground KD is diagonal in the frame of the quantization axes, and the principal components are

$$g^{1\text{-elec}}_X = g^{1\text{-elec}}_Y = \frac{2}{\sqrt{1+\frac{1}{\rho}}} \text{ and } g^{1\text{-elec}}_Z = 2 - \frac{2}{\sqrt{1+\rho}}, \quad (10)$$

where we have approximated the free-electron g-value as $g_e \approx 2$, and

$$\rho \equiv \frac{\Delta^2 + 4\eta^2}{\zeta^2}, \quad (11)$$

is an anisotropy parameter. The dependence of the principal components of the $\mathbf{g}$ tensor on ρ is plotted in Fig. 5.

There are three important limiting cases for the anisotropy barrier: (i) the isotropic limit where $\zeta = 0$ and Δ, $\eta \neq 0$ so that $\rho \to \infty$; (ii) the axial CF limit where $\zeta \neq 0$ and $\Delta = \eta = 0$ so that $\rho = 0$; and (iii) the strong-SOC limit where $\zeta^2 \gg \Delta^2 + 4\eta^2$ so that $\rho \approx 0$. Taking the respective limits of the elements $g^{1\text{-elec}}_X$, $g^{1\text{-elec}}_Y$ and $g^{1\text{-elec}}_Z$, we see that in the isotropic case (i) we recover the isotropic structure of the $\mathbf{g}$ tensor as expected: $g^{1\text{-elec}}_X = g^{1\text{-elec}}_Y = g^{1\text{-elec}}_Z = 2$. Cases (ii) and (iii) are otherwise equal

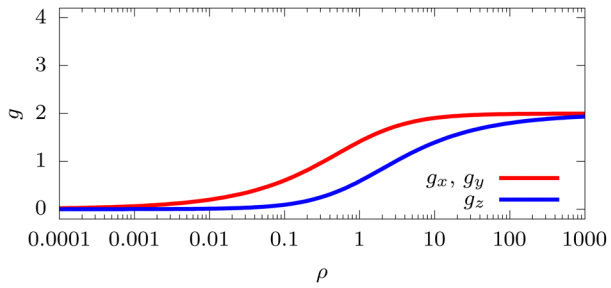

Fig. 5 Dependence of the principal components of the **g** tensor on the anisotropy parameter ρ in the np^1 case.

except case (iii) is approximate. In these cases $g_X^{1\text{-elec}} = g_Y^{1\text{-elec}} = g_Z^{1\text{-elec}} = 0$, which indicates that the ground state is diamagnetic. This follows from the perfect cancellation of the orbital magnetic moment projection $\mu_B m_l = \pm\mu_B$ on the quantization axis and the respective projection $2\mu_B m_s = \pm\mu_B$ of the spin magnetic moment. Since the system does not have a magnetic moment in its ground state in the strong SOC limit (iii), the np^1 configuration cannot lead to slow relaxation of magnetization.

4.4 np^2 case

In the two-electron case the basis states can be constructed by the application of a two-electron spin-tensor creation operator $\hat{Q}^{S,M_S}_{m_l,m_l'}$ that ensures that the resulting state is a spin eigenstate with a total spin S and spin projection M_S.[113,114] Choosing the basis states as spin eigenstates simplifies the structure of the Hamiltonian. A total of six basis states can be constructed:

$$\hat{Q}^{1,+1}_{-1,+1}|np^0\rangle,\quad \hat{Q}^{1,-1}_{-1,+1}|np^0\rangle,\quad \hat{Q}^{0,0}_{-1,+1}|np^0\rangle,\quad \hat{Q}^{1,0}_{-1,+1}|np^0\rangle,$$
$$\left(\hat{Q}^{0,0}_{-1,-1}+\hat{Q}^{0,0}_{+1,+1}\right)|np^0\rangle \quad\text{and}\quad \left(\hat{Q}^{0,0}_{-1,-1}-\hat{Q}^{0,0}_{+1,+1}\right)|np^0\rangle. \tag{12}$$

and the resulting matrix representation of the Hamiltonian is

$$H^{2\text{-elec}} = \begin{pmatrix} -K & 0 & 0 & 0 & 0 & 0 \\ 0 & -K & 0 & 0 & 0 & 0 \\ 0 & 0 & -K & \zeta & 0 & 0 \\ 0 & 0 & \zeta & K & -\Delta & 2i\eta \\ 0 & 0 & 0 & -\Delta & 0 & 0 \\ 0 & 0 & 0 & -2i\eta & 0 & 0 \end{pmatrix}. \tag{13}$$

The eigenvalues of the Hamiltonian (13) do not have simple analytical forms. However, assuming that the CF is much weaker than the SOC, Δ, $\eta \ll \zeta$, the CF can be introduced as a perturbation at the second order. Up to second order the eigenvalues are

$$E_1^{2\text{-elec}} = -K, \tag{14}$$
$$E_2^{2\text{-elec}} = -K, \tag{15}$$
$$E_3^{2\text{-elec}} = -\kappa - \left(1-\frac{K}{\kappa}\right)\cdot\frac{\Delta^2+4\eta^2}{2\kappa} + \mathcal{O}\left(\Delta^3,\eta^3\right), \tag{16}$$
$$E_4^{2\text{-elec}} = +\kappa + \left(1+\frac{K}{\kappa}\right)\cdot\frac{\Delta^2+4\eta^2}{2\kappa} + \mathcal{O}\left(\Delta^3,\eta^3\right), \tag{17}$$

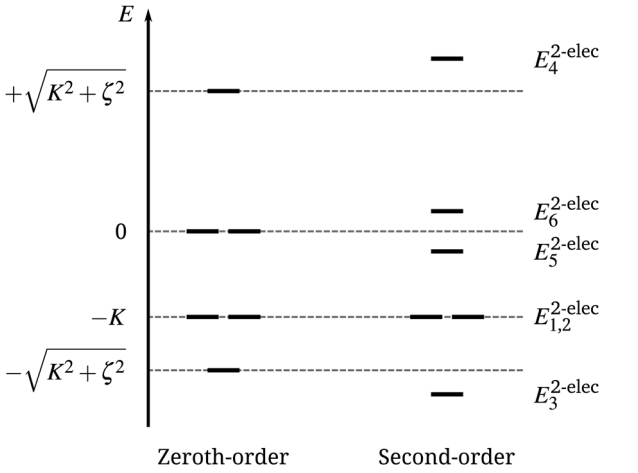

Fig. 6 Qualitative energy level diagram of the electronic states in the np^2 case calculated at the zeroth and second order of perturbation theory. The CF is treated as a perturbation and the zeroth-order energies include only the SOC and exchange interaction. The first-order perturbation correction does not affect the energies.

$$E_5^{2\text{-elec}} = -\frac{4K\eta^2}{\kappa^2} + \mathcal{O}\left(\Delta^3,\eta^3\right) \text{ and} \tag{18}$$

$$E_6^{2\text{-elec}} = +\frac{K\Delta^2}{\kappa^2} + \mathcal{O}\left(\Delta^3,\eta^3\right), \tag{19}$$

where $\kappa = \sqrt{K^2+\zeta^2}$. The first two eigenvalues $E_1^{2\text{-elec}}$ and $E_2^{2\text{-elec}}$ are exact as they correspond to the two 1×1 blocks of the Hamiltonian (13) while the four remaining values $E_3^{2\text{-elec}}$ to $E_6^{2\text{-elec}}$ are approximate eigenvalues of the 4×4 block.

The exchange integral K is always positive and all the remaining parameters ζ, Δ and η enter the eigenvalue expressions (14) as squares. Thus, $K \le \kappa$ and $0 \le K/\kappa \le 1$. Since we are assuming that the CF splitting within the np_x, np_y orbital space is weak, we can also assume $K \gg |\Delta|, |\eta|$. From these considerations, it can be concluded that $E_3^{2\text{-elec}}$ is the ground energy, $E_1^{2\text{-elec}} = E_2^{2\text{-elec}}$ are the first excited state. The energy level structure is visualized in Fig. 6. If the SOC vanishes so that $\zeta = 0$, then $\kappa = K$ and the ground state is a degenerate spin-triplet. The splitting between the ground state and the first excited state is of order ζ, that for the heavier main group elements is at least an order of magnitude larger than the thermal energy under ambient conditions. Thus, the ground state is an energetically isolated non-degenerate state. Due to Kramers' theorem[80,83] the non-degenerate state is diamagnetic. A diamagnetic ground state in a Bi(I) complex with an np^2 configuration has indeed been experimentally and quantum-chemically characterized.[63] Thus, the np^2 configuration cannot lead to slow relaxation of magnetization.

4.5 np^3 case

The three-electron case is easiest to treat by considering the particle-hole symmetry between the one-electron case, since in the three-electron case there is one hole in the otherwise fully occupied model orbital space. The basis states can then be constructed by using the one-electron spin-tensor operator $\hat{q}^{m_s}_{m_l}$

that creates a state with orbital momentum m_l and spin momentum m_s by annihilating one electron from the fully occupied np^4 orbital space.[115] The basis states are

$$\hat{q}_{-1}^{+1/2}|np^4\rangle,\ \hat{q}_{+1}^{+1/2}|np^4\rangle,\ \hat{q}_{+1}^{-1/2}|np^4\rangle \text{ and } \hat{q}_{-1}^{-1/2}|np^4\rangle, \tag{20}$$

and the Hamiltonian is

$$H^{3\text{-elec}} = \begin{pmatrix} K+\zeta/2 & -\gamma & 0 & 0 \\ -\gamma^* & K-\zeta/2 & 0 & 0 \\ 0 & 0 & K+\zeta/2 & -\gamma^* \\ 0 & 0 & -\gamma & K-\zeta/2 \end{pmatrix}. \tag{21}$$

The exchange integral K appears on all diagonal elements and can be removed by energy translation. The Hamiltonian (21) then becomes equivalent to the one-electron Hamiltonian (7) except with different signs on the off-diagonal elements. The three-electron Hamiltonian (21) has the same eigenvalues (8) and the same effective barrier height (9) as the one-electron Hamiltonian (7). Due to signs on the off-diagonal elements the eigenvectors in the one- and three-electron cases differ from each other. As a consequence, also the structure of the magnetic moment operators and **g** tensors is different. In the three-electron case, the principal components of the **g** tensor are

$$g_X^{3\text{-elec}} = g_Y^{3\text{-elec}} = \frac{2}{\sqrt{1+\frac{1}{\rho}}} = g_X^{1\text{-elec}} = g_Y^{1\text{-elec}} \text{ and}$$
$$g_Z^{3\text{-elec}} = 2 + \frac{2}{\sqrt{1+\rho}}, \tag{22}$$

where ρ is defined in eqn (11). The dependence of the principal components on ρ is plotted in Fig. 7.

In the isotropic limit when $\zeta = 0$, the **g** tensor reduces to the isotropic tensor $g_X^{3\text{-elec}} = g_Y^{3\text{-elec}} = g_Z^{3\text{-elec}} = 2$ like in the one-electron case. At the axial CF limit and the strong-SOC limit, the situation is, however, different. The transverse elements again vanish $g_X^{3\text{-elec}} = g_Y^{3\text{-elec}} = 0$, but the axial element tends to the value $g_Z^{3\text{-elec}} = 4$ unlike in the one-electron case. Thus, in the axial and strong-SOC limits, the **g** tensor has an ideal axial structure with $g_X = g_Y = 0$ and $g_Z \neq 0$. The value $g_Z^{3\text{-elec}} = 4$ also sets the ideal limit for a main-group SMM with a single heavy main-group atom or ion.

Slow relaxation of magnetization is, therefore, possible in a system with the np^3 configuration. Furthermore, it is the only np^N configuration where slow relaxation of magnetization can occur. An increase in both the SOC constant ζ and the CF parameters Δ and η leads to an increase in the value of U_{eff} that slows down the Orbach process and leads to a better SMM. However, only the increase of ζ leads to a more axial **g** tensor while increases in Δ and η lead to larger transverse elements g_X and g_Y. Commonly, slow relaxation of magnetization at zero fields can be observed in systems with transverse elements up to order g_X,$g_Y \sim 0.1$. Higher values of g_X and g_Y lead to efficient QTM and fast relaxation of magnetization at zero field.[116,117] At nonzero external or dipolar fields slow relaxation dynamics can still be observed with transverse elements up to order g_X,$g_Y \sim 0.7$.[118,119] It should be noted that the efficiency of QTM also depends on the nature and strength of the magnetic fields in the crystal lattice arising from dipolar and hyperfine interactions, and not only from g_X and g_Y. The transverse elements do, however, give a reasonable estimate.

The value $g_X = g_Y \sim 0.1$ is reached when $\Delta^2 + 4\eta^2 \sim 0.0025 \cdot \zeta^2$. Thus, an increase in the CF parameters Δ and η leads to the destruction of the magnetic axiality in the ground KD much quicker than they make a significant contribution to U_{eff}. The SOC constants of heavier p block elements can be estimated by observing the splitting of the ground ^2P terms of the heavier group 13 atoms with a one-electron np^1 configuration. In this case, the splitting approximately gives the value of ζ. The values for Ga, In and Tl are 826 cm^{-1}, 2213 cm^{-1} and 7793 cm^{-1}, respectively.[120–122] Thus, ζ can be taken to vary roughly from order $\sim$1000 cm^{-1} to order $\sim$8000 cm^{-1}. For a SOC constant ζ = 8000 cm^{-1}, the square-root magnitude $\sqrt{\Delta^2 + 4\eta^2}$ of the CF parameters should be less than $\sim$400 cm^{-1}, so that the transverse elements of the **g** tensor are less than $\sim$0.1. This is a very weak CF splitting indicating that even very small deviations from ideal molecular symmetries can quickly lead to a large increase in the transverse elements of the **g** tensor.

The values of U_{eff} and the principal components of the **g** tensor are plotted for various values of ζ as a function of the CF magnitude $\sqrt{\Delta^2 + 4\eta^2}$ as shown in Fig. 8. It is immediately clear from the figure that very large CF splitting is required in order to make a significant effect on U_{eff} whereas a much smaller value of $\sqrt{\Delta^2 + 4\eta^2}$ has an effect on the axiality of the **g** tensor. Thus, the results show that an ideal SMM requires minimal CF splitting in the np_x, np_y orbital space and maximal ζ. At this limit $\Delta^2 + 4\eta^2 \sim 0$ and $U_{\text{eff}} \sim \zeta$. This means that the effective barrier height in main-group SMMs is more or less directly determined by the SOC constant of the main-group element. The maximal possible value is then of the order $\sim$8000 cm^{-1}.

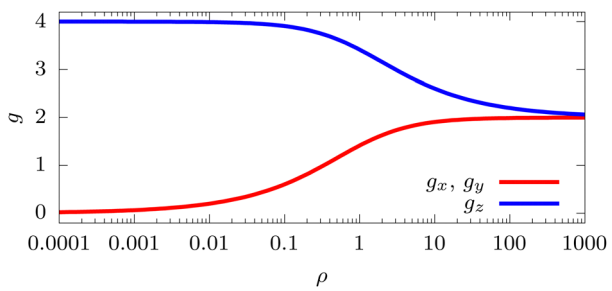

Fig. 7 Dependence of the principal components of the **g** tensor on the anisotropy parameter ρ in the np^3 case.

4.6 Validation of the model

In order to validate the theoretical model, the electronic structures of phenyl antimony PhSb and the respective cation and anion, $[PhSb]^+$ and $[PhSb]^-$, were calculated. In a cation, a neutral molecule and an anion, the Sb atom or ion has $5p^1$, $5p^2$ and $5p^3$ electron configurations, respectively. The antimony system was chosen as an example as it has a non-vanishing CF

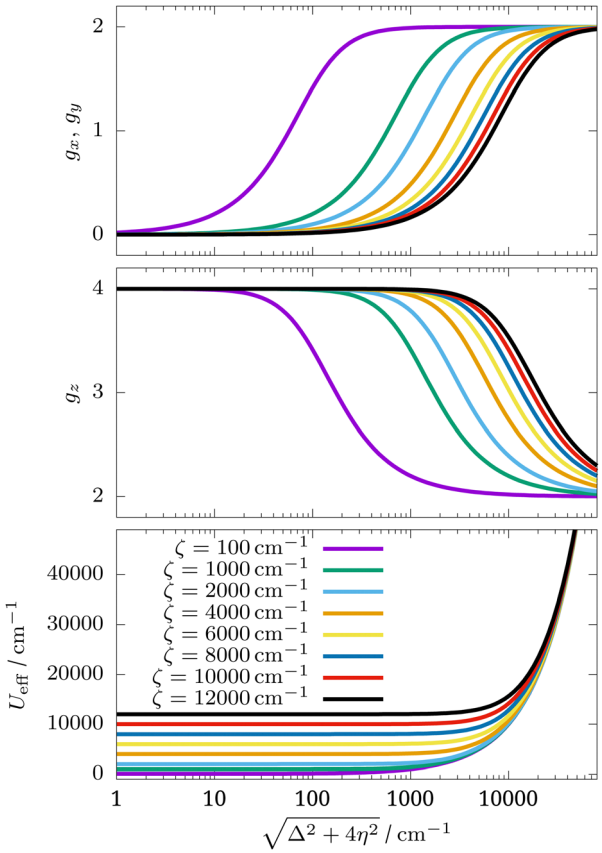

Fig. 8 Dependence of the principal components of the **g** tensor and the effective barrier height U_{eff} on the CF magnitude $\sqrt{\Delta^2 + 4\eta^2}$ at various values of the SOC constant ζ.

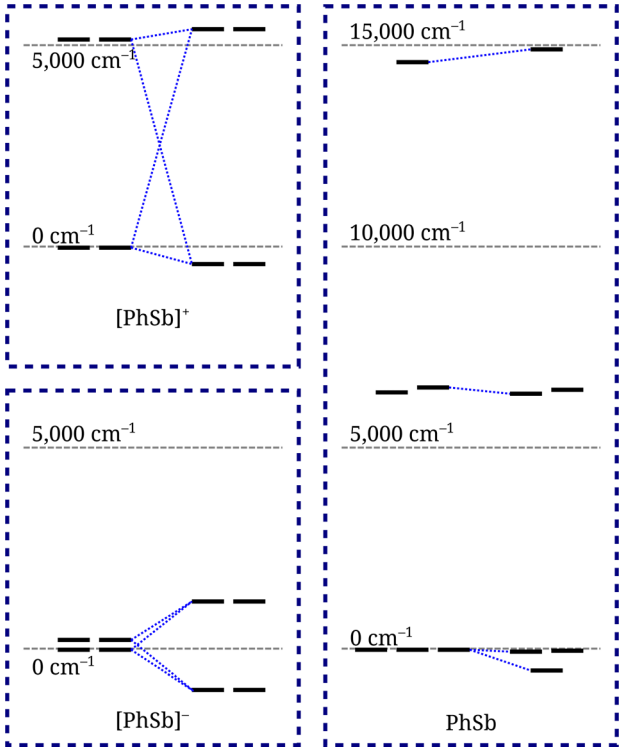

Fig. 9 Energy level structures of $[PhSb]^+$, PhSb and $[PhSb]^-$ calculated both with (right) and without (left) spin–orbit coupling.

splitting between the $5p_x$ and $5p_y$ orbitals and should, therefore, demonstrate most of the electronic structure features that fall into the domain of the theoretical model described in this section. Computational details are described in Sections S2.1 and S2.2 in the ESI.† The calculated energy level structures of $[PhSb]^+$, PhSb and $[PhSb]^-$ are shown in Fig. 9, and all agree well with the prediction of the model described in Section 4. In the case of the $5p^1$ system $[PhSb]^+$, the CF splitting is strong and, consequently, further splitting by SOC is relatively weak. In the case of the $5p^3$ anion $[PhSb]^-$, the CF splitting is weak and the two spin-doublets are almost degenerate before the inclusion of SOC, and split strongly under SOC to yield two KDs. In the case of both $[PhSb]^+$ and $[PhSb]^-$, the two KDs are the only states up to 15 000 cm^{-1}. In the case of the neutral $5p^2$ system PhSb, the ground spin state is a triplet that splits under SOC to yield a ground singlet state and an excited quasi doublet higher in energy. Within an energy range of 15 000 cm^{-1} there are three spin-singlet states that split weakly under SOC. The energy level structure closely follows the theoretical model.

In the case of $[PhSb]^+$ and $[PhSb]^-$ the energy difference between the two KDs can be directly associated with the effective energy barrier U_{eff} as defined in eqn (9). The energy splitting between the two spin doublets before the inclusion of SOC can be associated with U_{eff} at the limit $\zeta = 0$. Thus, this energy difference can be taken to be equal to the CF splitting $\sqrt{\Delta^2 + 4\eta^2}$. The value of ζ can then be calculated from the values of U_{eff} and $\sqrt{\Delta^2 + 4\eta^2}$. Similarly, the value of the anisotropy parameter ρ can be evaluated according to eqn (11), and the value of ρ can be used to calculate the principal components of the **g** tensor using (10) and (22). The **g** tensors can also be evaluated using the full *ab initio* magnetic moment operators following the implementation in the SINGLE_ANISO module.[41,42] Comparison of the **g** tensors calculated from the energy splitting of the KDs and the spin-doublets following the model, and from the full *ab initio* operators shows to what extent the assumptions and simplifications of the model effect the quantitative evaluation of the magnetic properties. The values are listed in Table 1. The *ab initio* and model-based **g** tensors agree rather well. The agreement is worse in the case of the cation $[PhSb]^+$ where also the CF splitting is large. The large value of the CF splitting means that the assumption of the CF as a weak perturbation on $5p_x$ and $5p_y$ is not fully realized, leading to some deviation between the fully *ab initio* and model predictions. In case of the anion $[PhSb]^-$, the CF splitting is weak and the agreement between the two **g** tensors is very good. Overall, the results show that the theoretical model provides a robust description of the magnetic properties as long as the CF splitting is not too strong. Most importantly, both the model and the *ab initio* calculations predict that the $5p^1$ configuration leads to a non-axial **g** tensors, the $5p^2$ configuration leads to a singlet ground state after the inclusion of SOC, and the $5p^3$ configuration leads to an axial **g** tensor.

Table 1 Main results of the validation study of the theoretical model

		[PhSb]$^+$	[PhSb]$^-$
Ab initio	$U_{\text{eff}}/\text{cm}^{-1}$	5834	2194
	$\sqrt{\Delta^2+4\eta^2}/\text{cm}^{-1}$	5169	245
	g_X	1.8433	0.2264
	g_Y	1.7704	0.2266
	g_Z	1.2700	3.9198
Calculated based on the model	ζ/cm^{-1}	2705	2181
	ρ	3.6529	0.0126
	g_X	1.7721	0.2232
	g_Y	1.7721	0.2232
	g_Z	1.0728	3.9875

5 Model structures

5.1 Target elements and oxidation states

Based on the conclusions made in Sections 3 and 4 the main-group atom or ion should have an np^3 configuration. The electron configuration determines the oxidation state of each p-block element depending on the group: group 13 elements should have the oxidation state −2, group 14 elements −1, group 15 elements 0, group 16 elements +1, group 17 elements +2 and group 18 elements +3. To get a comprehensive view of the heavier p-block elements we target elements at a rather loose criteria, and consider all 15 elements in the periods 4, 5 and 6 of the groups 13–17. Noble gas elements have been excluded due to their strong tendency to reduce other species in their positive oxidation states. The inherent radioactivity and scarcity of polonium and astatine, especially in the case of the latter, make their use in the construction and study of SMMs impractical. However, they have been included for completeness.

None of these oxidation states considered are the common oxidation states of the respective elements discussed in standard inorganic chemistry textbooks.[123–126] To the best of our knowledge, no structure has ever been isolated in the solid state where the main-group elements and oxidation states considered here are present as isolated atoms or ions bonded to a ligand framework by conventional covalent bonds. By isolated we mean that the main-group atom or ion E is not bonded to another similar atom or ion to form structures of the type E_n, where $n \geq 2$; and by conventional covalent bonds we mean that the main-group element is bonded to its ligand environment by localized covalent or coordination bonds, instead of multi-center bonding or cluster-like structures with features of metallic bonding. However, with the exception of polonium and astatine, all the elements and oxidation states considered in this work have been observed under some conditions. The elements of the groups 13 and 14 in oxidation states −2 and −1, respectively, have been characterized in Zintl phases.[127–129] The oxidation state 0 of the group 15 elements is present in stable isolated systems where a neutral E–E-moiety (E = As, Sb, Bi) has been stabilized by coordinated carbene ligands.[130–132] The oxidation state +1 of selenium and tellurium has been observed in the gas phase in the phenylselenyl and phenyltelluryl radicals, and the former has also been isolated in an argon matrix at liquid-helium temperature.[133,134] The +2 oxidation state of the group 17 halogens is present in the unstable gaseous radical monoxides BrO and IO that play roles in volcanic chemistry[135] and atmospheric chemistry,[136] respectively.

5.2 Target geometries

Based on the conclusions made in Sections 3 and 4 the chemical structures of main-group SMMs should be one- or two-coordinate complexes with at least local linearity around the main-group atom or ion. We considered a simple one-coordinate structure L–M (**1**), where M is the main-group atom and L is the ligand, a simple two-coordinate structure L–M–L (**2**) and a chloride salt L–M–Cl (**3**). The chloride ion was chosen to represent a relatively redox-inactive species with predominantly ionic metal–ligand bonding. Four ligands L were considered: a *tert*-butyl anion (**a**) representing a σ-donor where any metal–ligand π-bonding is minimal; a phenyl anion (**b**) representing a π-conjugated σ-donor where the main-group element may become involved in the π conjugation; an anionic bisilylamido ligand (**c**) that can act as a σ-donor and a π-donor; and a neutral N-heterocyclic carbene (NHC, **d**) ligand that can act as a σ-donor and a π-acceptor. The structures are summarized in Fig. 10. The structure labels consist of the element symbol, followed by a dash, a number representing the coordination geometry, and a lower-case letter representing the ligand. For example, the two-coordinate NHC complex of antimony is **Sb-2d**. A label **2d** refers to the two-coordinate NHC complex of any element, *etc.*

The model structures should be considered as the core moieties in the design of main-group SMMs. The unstable oxidation states and the unpaired electron require that the main-group element must be sterically protected by bulky groups. Such groups can be introduced as substituents to the core moiety. It should be noted that unlike in the case of many main-group radicals, the stabilization cannot be achieved by purely electronic means such as delocalization of the unpaired electron over the molecular skeleton[137,138] as the atom-like nature of the np_x and np_y orbitals is necessary for the magnetic anisotropy. The substituents do not affect the magnetic properties, at least at a qualitative level, as long as they are chosen in such a way that they do not lead to agostic or anagostic interactions with the main-group element that could lead to splitting of the np_x and np_y orbitals. However, in the case of heavier main-group elements, avoiding such detrimental

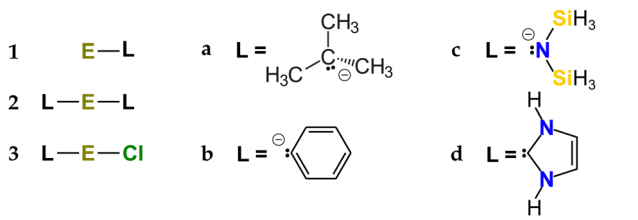

Fig. 10 Summary of the model structures. E is the main group element.

interactions is not trivial due to the very large spatial extent of the np_x and np_y orbitals. This issue will be discussed in more detail in Section 6.

5.3 Geometries and spin densities

The geometries of all the structures were fully optimized using density functional theory (DFT) without any symmetry constraints. The DFT calculations were carried out using the PBE exchange–correlation functional as implemented in the Amsterdam density functional (ADF) module[139,140] of the Amsterdam modeling suite (AMS) versions 2022.101 and 2023.101.[141] The computational details are described in Section S2.1 in the ESI.†

Based on the DFT calculations two criteria were set for the further consideration of a given structure: it should not dissociate and the unpaired electron should be localized on the main-group atom. Dissociated structure was defined as a structure where any of the metal–ligand bonds are greater than 5 Å, and the threshold for the selection based on spin density was set to 1 ± 0.1 unpaired electrons on the main-group atom. The calculated bond lengths and spin densities are listed in Tables S4 and S5 in the ESI,† and the spin densities are summarized in Fig. 11.

Most of the structures stay intact during geometry optimization. However, structures **3** dissociate for all group 13, 14 and 15 complexes except **Sb-3c**, **Bi-3c** and **Bi-3d**. In addition structures **1c**, **2a**, and **2c** of group 13 elements as well as structure **2c** of Sn and Pb dissociate. This is most likely due to the excessive negative charge on the complexes. All structures of group 16 and 17 elements except **Br-2d** remain intact. However, despite not dissociating in most structures, the unpaired electron does not stay on the main-group element in the majority of complexes considered. Due to the unstable oxidation states of the main-group elements, the complexes are prone to undergo intramolecular redox reactions where the unpaired spin is transferred to the ligand as a result of oxidation or reduction. This happens in all two-coordinate complexes **2** and **3** except in the two-coordinate bisilylamido complexes **2c** and **3c** of Sb and Bi. The remaining mono-coordinated complexes **1** are most stable in groups 14 and 15, where all monocoordinated complexes **1a–1d** have the correct spin density. In the other groups, only the butyl complex **1a** is redox-stable enough to retain the correct spin density. Complexes **1a** have the correct spin density for all elements considered except Br. In addition to these systems only complex **Tl-1d** has the correct spin density.

Thus, the chemical structures that can be considered should preferably be either mono-coordinated butyl complexes or mono-coordinated complexes of group 14 or 15 elements. The ligands should be highly resistant towards intramolecular redox reactions.

5.4 Energy-level structure and magnetic properties

The electronic structure and magnetic properties of structures that did not dissociate and had the correct spin density distribution were then calculated using multireference methods at the NEVPT2//CASSCF level[142–146] as implemented in the Orca code version 5.0.4.[147–149] Spin–orbit coupling effects were introduced using the quasi-degenerate perturbation theory (QDPT) approach.[43,150] The computational details are described in Section S2.2 in the ESI.†

The multireference wave functions of structures **In-1a**, **Tl-1a**, **Tl-1d**, **Pb-1a** and **Pb-1c** have excessively diffuse orbitals at the main-group element. Most likely the electrons are not bound, but due to the limits of the basis set approximation they cannot be removed into vacuum and instead the orbital optimization results into excessively diffuse orbitals. These structures were

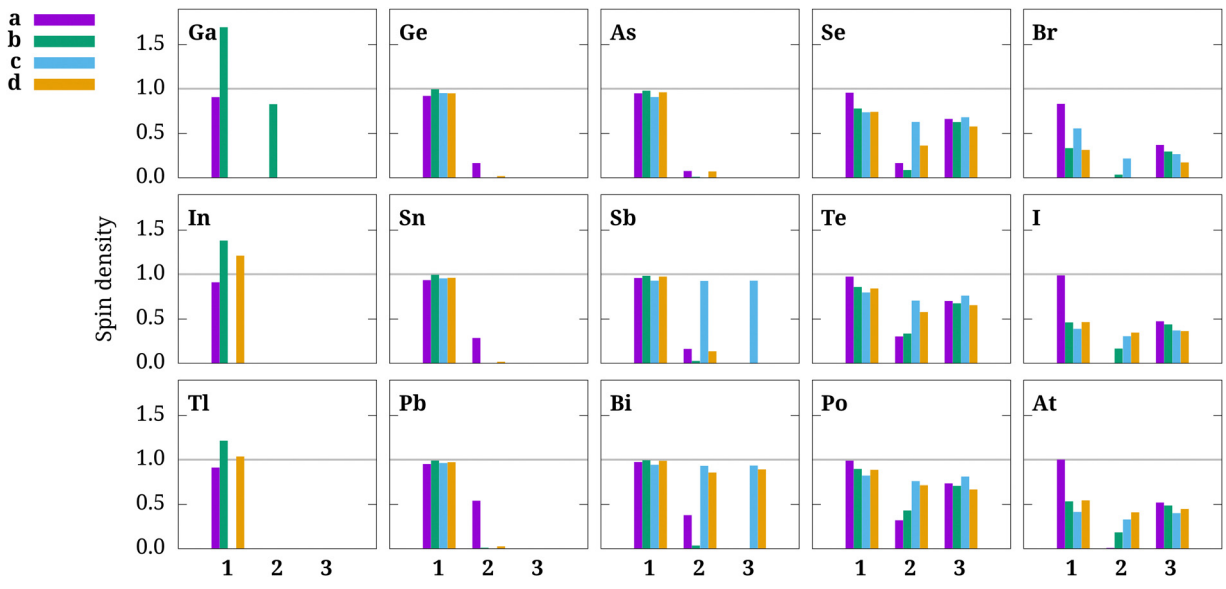

Fig. 11 QTAIM spin density calculated for the main-group element. Structures that dissociated upon geometry optimization are not included in the figure. The gray horizontal line indicates the value of 1.0 corresponding to one unpaired electron as expected for the np^3 case.

Table 2 Main results of the multireference calculations

	$\sqrt{\Delta^2+4\eta^2}/\mathrm{cm}^{-1}$ [a]	$U_{\mathrm{eff}}/\mathrm{cm}^{-1}$ [b]	g_X	g_Y	g_Z	ζ/cm^{-1} [c]	ρ [c]
Ga-1a	55	227	0.4834	0.4842	3.9151	220	0.0634
Ge-1a	111	529	0.4192	0.4194	3.9099	517	0.0457
Ge-1c	3230	3276	1.9721	1.9721	2.3255	545	35.1108
Ge-1d	6478	6486	1.9947	1.9953	2.0845	329	387.6244
Sn-1a	55	975	0.1137	0.1138	3.9722	973	0.0032
Sn-1b	402	1056	0.7641	0.7657	3.8069	977	0.1695
Sn-1c	1273	1711	1.4871	1.4871	3.3099	1144	1.2375
Sn-1d	1749	2083	1.6767	1.6862	2.9838	1130	2.3939
Pb-1b	344	3280	0.2137	0.2142	3.9543	3262	0.0111
Pb-1d	767	3833	0.3870	0.3886	3.8557	3756	0.0417
As-1a	176	1013	0.3491	0.3495	3.9187	998	0.0311
As-1b	1535	1810	1.6940	1.6945	2.9806	959	2.5630
As-1c	3603	3746	1.9235	1.9235	2.5354	1025	12.3607
As-1d	1722	1963	1.7503	1.7504	2.8700	943	3.3357
Sb-1a	120	2205	0.1104	0.1105	3.9591	2201	0.0030
Sb-1b	221	2192	0.2043	0.2046	3.9238	2181	0.0102
Sb-1c	2429	3367	1.4418	1.4418	3.3586	2332	1.0852
Sb-1d	535	2361	0.4430	0.4430	3.8440	2300	0.0542
Sb-2c	2408	3365	1.4311	1.4312	3.3722	2350	1.0492
Sb-3c	1725	2920	1.1857	1.1898	3.5917	2357	0.5359
Bi-1a	88	6522	0.0283	0.0283	4.0291	6521	0.0002
Bi-1b	35	6471	0.0149	0.0151	3.9568	6471	0.0000
Bi-1c	1835	7423	0.4910	0.4910	3.9118	7192	0.0651
Bi-1d	135	7161	0.0163	0.0163	3.9296	7160	0.0004
Bi-2c	1963	7933	0.5384	0.5438	4.1069	7686	0.0652
Bi-3c	1206	9197	0.1965	0.2021	4.0580	9118	0.0175
Se-1a	298	1624	0.3715	0.3726	3.9148	1597	0.0348
Te-1a	173	3528	0.1008	0.1009	3.9656	3524	0.0024
Po-1a	127	9817	0.0256	0.0261	3.9834	9816	0.0002
I-1a	194	3829	0.1067	0.1075	3.9807	3824	0.0026
At-1a	136	6247	0.0384	0.0386	4.0243	6245	0.0005

[a] Energy difference between the two lowest-energy spin doublets before the inclusion of SOC. [b] Energy difference between the two lowest-energy doublets after the inclusion of SOC. [c] Calculated from the values of $\sqrt{\Delta^2+4\eta^2}$ and U_{eff}.

eliminated from further calculations. In the case of In and Tl this most likely results from the excessive negative charge on the rather electropositive elements. This is most likely also the reason for the excessively diffuse orbitals in **Pb-1a** and **Pb-1c**; however, it appears that the metal–ligand π-conjugation that is possible in **Pb-1b** and **Pb-1d** manages to stabilize the large negative charge on the Pb ion. Similarly diffuse orbitals were not observed in the lighter group 14 elements Ge and Sn. The structures **In-1a**, **Tl-1a**, **Tl-1d**, **Pb-1a** and **Pb-1c** were not included in any further analyses. The magnetic properties of **Ge-1b** could not be calculated due to the strong CF splitting as compared to SOC that would lead to an imaginary SOC constant when calculated according to the procedure described in Section 4.6. This unphysical situation arises because the theoretical model breaks down in the presence of strong CF interaction bordering on covalency. Thus, **Ge-1b** was also excluded from further analysis.

The results of the multireference calculations are summarized in Table 2. From an electronic-structure point of view, the prospects of a given structure displaying SMM behavior can be estimated on the basis of the magnetic axiality of the ground KD and the height of the effective barrier U_{eff}. In a highly axial KD, the anisotropy parameter ρ is close to zero. A value of $\rho = 0.001$ leads to $g_X = g_Y \sim 0.06$, which can be considered to be close to the upper limit of g_X and g_Y where SMM properties can still be observed at zero magnetic fields. The only structures that fulfill these criteria are **Bi-1a**, **Bi-1b**, **Bi-1d**, **Po-1a** and **At-1a**. In terms of the axiality of the **g** tensor, the best structure is **Bi-1b**. The structure **Po-1a** gives the highest U_{eff} at 9817 cm^{-1}. However, while both **Po-1a** and **At-1a** are good candidates from a purely electronic-structure point of view, the radioactivity of Po makes it an impractical system, and the intense radioactivity and extreme scarcity of At make it a purely theoretical consideration. Thus, the most likely route towards main-group SMMs is based on Bi. Reasonable alternatives with high but less than ideal axiality are **Te-1a** and **Sb-1a**.

5.5 Discussion

In the case of all but the heaviest of p-block elements, the axiality of the **g** tensor is broken in one way or the other leading to nonzero transverse components in the **g** tensor that make QTM highly efficient. This is not unexpected as the p-orbitals in general have a very high tendency to form covalent bonds. While from a chemical-structure and reactivity points of view, the heavier p-block elements rarely form multiple bonds,[108,109,125,151] from a magnetism point of view even very small covalency contributions that do not have a local σ-symmetry lead to unequal interactions between the $n\mathrm{p}_x$ and

np_y orbitals that split and mix the orbitals giving a nonzero CF splitting $\sqrt{\Delta^2 + 4\eta^2}$. This then ultimately leads to the transverse components in the **g** tensor.

It is clear from the results shown in Table 2 that the general trend is that the CF splitting decreases as one moves down a group, and at the same time SOC increases. The increase in SOC is not surprising as the one-electron SOC-integral is proportional to the fourth power of the nuclear charge and is much larger for heavy elements than the lighter ones.[112] The calculated SOC integrals ζ vary between 200 cm^{-1} and 1600 cm^{-1} in period 4, between 900 cm^{-1} and 3900 cm^{-1} in period 5 and between 3200 cm^{-1} and 10 000 cm^{-1} in period 6, increasing from left to right in each period. The decrease in the CF splitting in the heavier elements is contrary to what is observed in the d-block where the 4d and 5d metals have considerably stronger CF splitting than the 3d metals.[83,96] The simplest explanation for the decrease in the CF splitting is the increased spatial extent of the p-orbitals. This leads both to longer metal–ligand σ-bonds due to the increased size of the relevant orbitals, and stronger σ-component in the bond due to the increased overlap of the np_z-orbital with the ligand σ-donating orbitals. At the same time, the overlap of the np_x and np_y orbitals and the ligand orbitals is reduced due to the longer bond length, leading to the weakening of any π-component in the bond. Therefore, an increase in the p-orbital size leads to the simultaneous strengthening of the σ-bond and weakening of any π-bonds. Since the strength of the σ-bond plays no role in the CF model, the only observed feature is the reduced CF-splitting due to the reduced π interaction. This effect is most clearly present in the structures **1b** and **1d** of group 14 and 15 elements. Especially in the case of group 15 **1b** structures, the CF splitting is reduced by an order of magnitude in each period. The effect is less pronounced in the structure **1a** where the CF splitting is weak in all structures due to the purely σ-donor ligand. It should be noted that the decrease of the CF splitting cannot be explained by the "inert-pair effect",[97–99] as s-orbitals do not play a significant role in the magnetic properties or bonding. Neither can it be explained by the formation of an inert pair in the spin–orbit coupled $np_{1/2}$ one-electron energy level,[97,152] as the CF effect is present already at a scalar-relativistic level.

It is only in the heaviest p-block elements in period 6, where the SOC is strong enough and the CF splitting is weak enough, so that ζ is much larger than $\sqrt{\Delta^2 + 4\eta^2}$, and the anisotropy parameter ρ approaches zero according to eqn (11). In the case of the earlier period 6 p-block elements, Tl and Pb, the negative charge on the main-group element necessary for the correct electronic configuration makes the electronic structure too unstable. The next elements, Bi, Po and At, are the ideal elements from an electronic-structure point of view, while only Bi is feasible from a practical point of view. The last period 6 element, Rn, was not considered in the present work due to the unlikeliness of the noble gas existing in the necessary +3 oxidation state and due to its inherent radioactivity.

6 Realistic structures

6.1 Target structures

Based on the results of Sections 4 and 5, the most promising chemical structure of a main-group SMM is a mono-coordinated Bi(0) complex where the Bi atom is bonded to the ligand with a single covalent bond. Such a system will need considerable steric protection around the Bi atom to avoid dimerization and other possible reactivity. It is expected that the relatively electropositive Bi in the low oxidation state is a strong oxidant. To the best of our knowledge, no such structure has ever been characterized. Herein we will consider two anion structures based on the phenylbismuth anion **Bi-1b** with bulky substituents added to the phenyl skeleton. The structures, $[\mathbf{4}]^-$ and $[\mathbf{5}]^-$, are shown in Fig. 12.

The neutral bismuthinidene **4** with a $6p^2$ configuration has been experimentally characterized.[63] The structure of **4** is based on a hydrindacene ligand with bulky substituents.[153] The same ligand has recently been used to successfully stabilize various compounds with mono-coordinated main-group elements in unusual oxidation states including a germylene radical,[68] a nitrene in a spin-triplet state[69] and a gallanediyl.[70] **4** has a triplet spin ground state that is strongly split under SOC to produce an overall singlet ground state as discussed in Section 4. It is remarkably stable and can be isolated in gram quantities. The hypothetical anion $[\mathbf{4}]^-$ with a $6p^3$ configuration can be obtained from **4** with a hypothetical one-electron reduction. The hypothetical anion $[\mathbf{5}]^-$ is based on the C_6H-2,6-$(C_6H_2$-2,4,6-$iPr_3)_2$-3,5-iPr_2 ligand which has previously been used to stabilize a highly reactive one-coordinate Al(I) compound.[65] The $[\mathbf{5}]^-$ anion with a $6p^3$ configuration can be obtained from the likewise hypothetical neutral bismuthinidene **5** with a $6p^2$ configuration.

6.2 Results

The geometries and energy-level structure of **4**, $[\mathbf{4}]^-$, **5** and $[\mathbf{5}]^-$ were calculated at the same level of theory as in the case of the model geometries as described in Sections S2.1 and S2.2 of the ESI.† Reduction potentials were calculated using a compound method utilizing DFT single-point calculations, multireference energy-level structure, and single-point calculations at DLPNO-

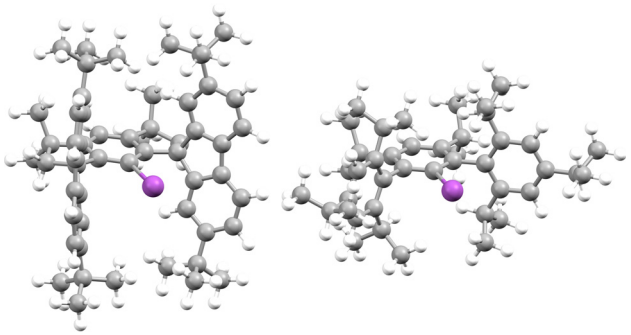

$[\mathbf{4}]^-$ $[\mathbf{5}]^-$

Fig. 12 Optimized geometries of the hypothetical sterically protected anions $[\mathbf{4}]^-$ and $[\mathbf{5}]^-$.

Table 3 Main properties calculated for the hypothetical sterically protected anions $[\mathbf{4}]^-$ and $[\mathbf{5}]^-$

		$[\mathbf{4}]^-$	$[\mathbf{5}]^-$
Ab initio	$U_{\text{eff}}/\text{cm}^{-1}$	7285	7471
	$\sqrt{\Delta^2+4\eta^2}\big/\text{cm}^{-1}$	2443	2783
	g_X	0.6796	0.7561
	g_Y	0.6938	0.7711
	g_Z	3.6925	3.6621
Calculated based on the model	ζ/cm^{-1}	6863	6933
	ρ	0.1267	0.1611
	g_X	0.6706	0.7450
	g_Y	0.6706	0.7450
	g_Z	3.8842	3.8560

CCSD(T) level[154–158] as implemented in Orca version 5.0.4.[147–149] Details of the reduction potential calculation are given in Section S2.3 in the ESI.†

The reduction potentials calculated for **4** and **5** are −1.9 V and −2.0 V *versus* the standard hydrogen electrode (SHE), respectively. The values are higher than the reduction potential of the simple compound PhBi calculated as −1.5 V in earlier work,[72] and it is important to note that accurate calculation of reduction potentials is often challenging.[159] The calculated potentials do, however, give a general idea of the stability and accessibility of the anions $[\mathbf{4}]^-$ and $[\mathbf{5}]^-$. The values are high but still within the solvent potential window, and should be within the scope of redox chemistry. The large negative potential does, however, mean that the systems are strong oxidants. This emphasizes the need for steric protection of the Bi atom and also places limits on the chemical nature of the ligands; *i.e.*, the ligands need to be resistant towards oxidation.

The parameters describing the magnetic properties of $[\mathbf{4}]^-$ and $[\mathbf{5}]^-$ are listed in Table 3. The predicted effective barrier heights U_{eff} are 7285 cm^{-1} and 7471 cm^{-1} for $[\mathbf{4}]^-$ and $[\mathbf{5}]^-$, respectively. The values are four times as high as the highest barriers of 1687 cm^{-1} and 1843 cm^{-1} that have been determined by fits to magnetic relaxation data measured on an experimentally characterized system.[160,161] The barrier is also higher than the barrier of 6471 cm^{-1} calculated for the simple complex **Bi-1b**. The increased barrier results from the CF splitting $\sqrt{\Delta^2+4\eta^2}$ that is over two orders of magnitudes larger in both $[\mathbf{4}]^-$ and $[\mathbf{5}]^-$ when compared to **Bi-1b**. However, due to the stronger CF splitting the anisotropy parameter ρ is four orders of magnitude larger in both complexes $[\mathbf{4}]^-$ and $[\mathbf{5}]^-$ as compared to **Bi-1b**. As a result, the magnetic state is considerably less axial, and there are significant transverse elements g_X and g_Y of the order $\sim$0.7 in the **g** tensor. The transverse elements are large enough to enable highly efficient QTM at zero field while still small enough that slow relaxation of magnetization most likely can be observed in the presence of a magnetic field. The field can be either external to the sample or originate from dipolar interaction between the magnetic moments of different metal atoms or ions in the crystal lattice.

The reduced axiality of $[\mathbf{4}]^-$ and $[\mathbf{5}]^-$ as compared to **Bi-1b** results from the interaction between the bulky flanking groups of the ligands with the Bi atom. The shortest non-bonding Bi–C contacts in the optimized structures of $[\mathbf{4}]^-$ and $[\mathbf{5}]^-$ are 3.419 Å and 3.381 Å, respectively. The respective sum of van der Waals radii is 3.77 Å[162,163] while the sum of computed covalent radii is 2.26 Å.[164] Thus, the close contacts clearly fall into the region of non-covalent interactions. The large spatial extent of the $6p_x$ and $6p_y$ orbitals means that this interaction leads to large crystal-field splitting of the orbitals, and considerably reduced magnetic axiality. This introduces considerable challenges in the chemical design and synthetic preparation of main-group SMMs.

6.3 Discussion

The synthetic problem both in the case of main-group SMMs proposed in this work and in the case of lanthanide SMMs is ultimately rather similar: how to stabilize low-coordinate systems without disturbing the magnetic axiality of the metal ion by detrimental metal–ligand interactions. In the case of lanthanide SMMs, the synthesis of low-coordinate complexes with minimal non-covalent metal–ligand interactions has long been a goal in the synthesis of new SMMs,[38,87] and recently important advances have been made in the synthesis of formally two-coordinate lanthanide SMMs.[119,165,166] Mono-coordinate lanthanide SMMs, however, are still confined to theoretical and computational work.[39,167] Trivalent lanthanide ions have the advantage that the strongly contracted 4f orbitals are effectively protected from detrimental metal–ligand interactions by the fully occupied 5s and 5p shells. It has been shown, for example, that in the case of a two-coordinate Yb(III) complex rather short non-bonding Yb–ligand interactions lead only to a relatively small deterioration of the magnetic anisotropy.[119] Similar conclusions have also been made in the case of a two-coordinate Dy(III) complex.[166] In case of the main-group systems, the synthetic problem is, however, made much more challenging due to the larger spatial extent and minimal electronic protection of the np_x and np_y orbitals. Furthermore, in the main-group SMMs the main-group elements are in a chemically unstable oxidation state whereas in lanthanide SMMs the lanthanide ion is usually in the ubiquitous and redox-stable trivalent oxidation state.

The main design criteria for the ligands are as follows: (i) the ligand should provide a sufficient steric bulk to protect the main-group element; (ii) the ligand should have only minimal non-covalent interactions with the main-group element; and (iii) the ligand should be resistant towards oxidation and other possible reactivity with the main-group element. The structures $[\mathbf{4}]^-$ and $[\mathbf{5}]^-$ should allow sufficient axiality to display slow relaxation of the magnetization in the presence of a magnetic field but not at zero field. Any hysteresis, if observable at all, would be strongly waist-restricted. The structures can be used as a starting point to design ligands that would better fulfill criteria (ii) and would then lead to stronger axiality and main-group SMMs at zero fields. Possible modification of the structure should be such that the angle between the two flanking hydrindacene groups (in the case of $[\mathbf{4}]^-$) or the arene groups (in the case of $[\mathbf{5}]^-$) is increased to reduce the short contacts between the flanking groups and the Bi atom. This could be

achieved, for example, by adding further steric bulk to the substituents on the flanking groups. However, choosing the correct substituents is not trivial as they could possibly allow new interactions with the Bi atom or reduce the angle between the flanking groups due to the increased dispersion attraction between them as has been shown to happen with bulky substituents.[151,168] Groups other than hydrocarbons could also be considered but it is important to choose them in such a way that they do not violate criteria (iii).

7 Conclusions

The possibility of designing a new generation of SMMs based on main-group elements was studied. Based on qualitative electronic-structure considerations, the most likely candidates were chosen as mono- or two-coodinated monometallic complexes of the main-group elements. A theoretical model was constructed to demonstrate that an electronic structure capable of displaying SMM behavior is only possible with an np^3 electronic configuration. A large number of possible p-block elements in various monometallic one- and two-coordinate model geometries were studied. The results show that only mono-coordinated structures form a good basis for the realization of SMMs. While there is nothing fundamental that forbids two-coordinate structures from being used, all of the two-coordinate structures are considered either dissociated or lead to some internal redox reaction of the main-group element that then lead to an undesirable oxidation state and/or delocalization of the spin. The results further show that only in the case of the heaviest p-block elements the SOC is strong enough to overcome the CF effects on the np_x and np_y orbitals. The CF effects that arise from the metal–ligand interaction are detrimental to the magnetic axiality of the ground state that is an essential requirement for an SMM. The axiality, as measured by the smallness of the transverse elements of the $\mathbf{g}$ tensor calculated for the ground doublet, increases with increasing SOC and decreases with increasing CF. In case of the lighter p-block elements, the SOC is not strong enough to overcome the negative effects of the CF. Both the SOC and the CF contribute positively to the effective barrier height U_{eff}.

Of the 6p elements bismuth in the oxidation state 0 provides the best starting point for the design of main-group SMMs; namely, its radioactivity plays no role in its chemistry, and the electronic structure of its complexes in the zerovalent oxidation state is not too unstable. Practical realization of SMMs based on Bi(0) is, however, challenging. Two possible structures with bulky steric groups protecting the Bi atom were proposed. The systems show high effective barriers measuring 7285 cm^{-1} and 7471 cm^{-1}, which are four times as high as the highest barrier observed on an experimentally characterized SMM.[160,161] However, the magnetic axiality is severely reduced by the interaction of the steric groups with the Bi atom affording possible slow relaxation of magnetization most likely only in the presence of an external magnetic field.

The present work shows that main-group SMMs are plausible and establishes a general framework for their chemical and electronic structures. The results further show that the effective barriers of main-group SMMs for the reversal of magnetization can greatly surpass those of even the best-performing f-block SMMs. However, the magnetic relaxation dynamics in SMMs are not determined purely by the effective barrier,[47,54,55,93,169] and their existence can ultimately only be validated by experiment. Thus, the experimental realization of a main-group system that functions as an SMM at zero fields is still an open challenge that needs to be further studied both from theoretical and experimental points of view.

Author contributions

A. M.: conceptualization, formal analysis, funding acquisition, investigation, methodology, project administration, resources, supervision, validation, visualization, writing – original draft and writing – review & editing; A. C. P.: formal analysis and investigation.

Data availability

The data supporting this article have been included as part of the ESI.†

Conflicts of interest

There are no conflicts to declare.

Acknowledgements

Financial support was provided by the Academy of Finland (project 332294) and the University of Oulu (Kvantum Institute). Computational resources were provided by the CSC-IT Center for Science in Finland and the Finnish Grid and Cloud Infrastructure (persistent identifier urn:nbn:fi:research-infras-2016072533).

Notes and references

1 R. Sessoli, D. Gatteschi, A. Caneschi and M. A. Novak, *Nature*, 1993, **365**, 141–143.
2 D. Gatteschi, R. Sessoli and J. Villain, *Molecular Nanomagnets*, Oxford University Press, Oxford, UK, 2006.
3 C. Benelli and D. Gatteschi, *Introduction to Molecular Magnetism. From Transition Metals to Lanthanides*, Wiley-VCH, Weinheim, Germany, 2015.
4 S. T. Liddle and J. van Slageren, *Chem. Soc. Rev.*, 2015, **44**, 6655–6669.
5 C. Godfrin, A. Ferhat, R. Ballou, S. Klyatskaya, M. Ruben, W. Wernsdorfer and F. Balestro, *Phys. Rev. Lett.*, 2017, **119**, 187702.
6 M. N. Leuenberger and D. Loss, *Nature*, 2001, **410**, 789–793.
7 L. Bogani and W. Wernsdorfer, *Nat. Mater.*, 2008, **7**, 179–186.

8 M. Urdampilleta, S. Klyatskaya, J.-P. Cleuziou, M. Ruben and W. Wernsdorfer, *Nat. Mater.*, 2011, **10**, 502–506.
9 A. Ghirri, A. Candini and M. Affronte, *Magnetochemistry*, 2017, **3**, 12.
10 A. Gaita-Ariño, F. Luis, S. Hill and E. Coronado, *Nat. Chem.*, 2019, **11**, 301–309.
11 M. Atzori and R. Sessoli, *J. Am. Chem. Soc.*, 2019, **141**, 11339–11352.
12 A. Chiesa, P. Santini, E. Garlatti, F. Luis and S. Carretta, *Rep. Prog. Phys.*, 2024, **87**, 034501.
13 R. Sessoli, H. L. Tsai, A. R. Schake, S. Wang, J. B. Vincent, K. Folting, D. Gatteschi, G. Christou and D. N. Hendrickson, *J. Am. Chem. Soc.*, 1993, **115**, 1804–1816.
14 N. Ishikawa, M. Sugita, T. Ishikawa, S.-Y. Koshihara and Y. Kaizu, *J. Am. Chem. Soc.*, 2003, **125**, 8694–8695.
15 N. Ishikawa, M. Sugita, T. Ishikawa, S.-Y. Koshihara and Y. Kaizu, *J. Phys. Chem. B*, 2004, **108**, 11265–11271.
16 D. N. Woodruff, R. E. P. Winpenny and R. A. Layfield, *Chem. Rev.*, 2013, **113**, 5110–5148.
17 *Lanthanides and Actinides in Molecular Magnetism*, ed. R. A. Layfield and M. Murugesu, Wiley-VCH, Weinheim, Germany, 2015.
18 J.-L. Liu, Y.-C. Chen and M.-L. Tong, *Chem. Soc. Rev.*, 2018, **47**, 2431–2453.
19 A. Dey, P. Kalita and V. Chandrasekhar, *ACS Omega*, 2018, **3**, 9462–9475.
20 Z. Zhu and J. Tang, *Natl. Sci. Rev.*, 2022, nwac194.
21 K. R. Meihaus and J. R. Long, *Dalton Trans.*, 2015, **44**, 2517–2528.
22 J. M. Frost, K. L. M. Harriman and M. Murugesu, *Chem. Sci.*, 2016, **7**, 2470–2491.
23 M. Feng and M.-L. Tong, *Chem. – Eur. J.*, 2018, **24**, 7574–7594.
24 L. Escalera-Moreno, J. J. Baldoví, A. Gaita-Ariño and E. Coronado, *Inorg. Chem.*, 2019, **58**, 11883–11892.
25 F.-S. Guo, B. M. Day, Y.-C. Chen, M.-L. Tong, A. Mansikkamäki and R. A. Layfield, *Science*, 2018, **362**, 1400–1403.
26 C. A. P. Goodwin, F. Ortu, D. Reta, N. F. Chilton and D. P. Mills, *Nature*, 2017, **548**, 439–442.
27 K. R. McClain, C. A. Gould, K. Chakarawet, S. J. Teat, T. J. Groshens, J. R. Long and B. G. Harvey, *Chem. Sci.*, 2018, **9**, 8492–8503.
28 J. D. Rinehart, M. Fang, W. J. Evans and J. R. Long, *J. Am. Chem. Soc.*, 2011, **133**, 14236–14239.
29 S. Demir, M. I. Gonzalez, L. E. Darago, W. J. Evans and J. R. Long, *Nat. Commun.*, 2017, **8**, 2144.
30 N. Mavragani, D. Errulat, D. A. Gálico, A. A. Kitos, A. Mansikkamäki and M. Murugesu, *Angew. Chem., Int. Ed.*, 2021, **60**, 24206–24213.
31 H.-D. Li, S.-G. Wu and M.-L. Tong, *Chem. Commun.*, 2023, **59**, 6159–6170.
32 F. Liu, D. S. Krylov, L. Spree, S. M. Avdoshenko, N. A. Samoylova, M. Rosenkranz, A. Kostanyan, T. Greber, A. U. B. Wolter, B. Büchner and A. A. Popov, *Nat. Commun.*, 2017, **8**, 16098.
33 C. A. Gould, K. R. McClain, D. Reta, J. G. C. Kragskow, D. A. Marchiori, E. Lachman, E.-S. Choi, J. G. Analytis, R. D. Britt, N. F. Chilton, B. G. Harvey and J. R. Long, *Science*, 2022, **375**, 198–202.
34 K. R. McClain, H. Kwon, K. Chakarawet, R. Nabi, J. G. C. Kragskow, N. F. Chilton, R. D. Britt, J. R. Long and B. G. Harvey, *J. Am. Chem. Soc.*, 2023, **145**, 8996–9002.
35 H. Kwon, K. R. McClain, J. G. C. Kragskow, J. K. Staab, M. Ozerov, K. R. Meihaus, B. G. Harvey, E. S. Choi, N. F. Chilton and J. R. Long, *J. Am. Chem. Soc.*, 2024, **146**, 18714–18721, in press.
36 J. D. Rinehart and J. R. Long, *Chem. Sci.*, 2011, **2**, 2078–2085.
37 F. Neese and D. A. Pantazis, *Faraday Discuss.*, 2011, **148**, 229–238.
38 N. F. Chilton, *Inorg. Chem.*, 2015, **54**, 2097–2099.
39 L. Ungur and L. F. Chibotaru, *Inorg. Chem.*, 2016, **55**, 10043–10056.
40 V. Vieru, S. Gómez-Coca, E. Ruiz and L. F. Chibotaru, *Angew. Chem., Int. Ed.*, 2024, **63**, e202303146.
41 L. F. Chibotaru and L. Ungur, *J. Chem. Phys.*, 2012, **137**, 064112.
42 L. Ungur and L. F. Chibotaru, in *Lanthanides and Actinides in Molecular Magnetism*, ed. R. A. Layfield and M. Murugesu, Wiley-VCH, Weinheim, Germany, 2015, pp. 153–184.
43 M. Atanasov, D. Aravena, E. Suturina, E. Bill, D. Maganas and F. Neese, *Coord. Chem. Rev.*, 2015, **289–290**, 177–214.
44 M. Atanasov, D. Ganyushin, K. Sivalingam and F. Neese, in *Molecular Electronic Structures of Transition Metal Complexes II*, ed. D. M. P. Mingos, P. Day and J. P. Dahl, Springer, Berlin, Germany, 2012, pp. 149–220.
45 L. Ungur and L. F. Chibotaru, *Chem. – Eur. J.*, 2017, **23**, 3708–3718.
46 K. L. M. Harriman, D. Errulat and M. Murugesu, *Trends Chem.*, 2019, **1**, 425–439.
47 A. Lunghi, F. Totti, R. Sessoli and S. Sanvito, *Nat. Commun.*, 2017, **8**, 14620.
48 A. Lunghi, F. Totti, S. Sanvito and R. Sessoli, *Chem. Sci.*, 2017, **8**, 6051–6059.
49 M. Briganti, F. Santanni, L. Tesi, F. Totti, R. Sessoli and A. Lunghi, *J. Am. Chem. Soc.*, 2021, **143**, 13633–13645.
50 A. Lunghi, *Sci. Adv.*, 2022, **8**, eabn7880.
51 S. Mondal and A. Lunghi, *J. Am. Chem. Soc.*, 2022, **144**, 22965–22975.
52 D. Reta, J. G. C. Kragskow and N. F. Chilton, *J. Am. Chem. Soc.*, 2021, **143**, 5943–5950.
53 R. Nabi, J. K. Staab, A. Mattioni, J. G. C. Kragskow, D. Reta, J. M. Skelton and N. F. Chilton, *J. Am. Chem. Soc.*, 2023, **145**, 24558–24567.
54 L. Gu and R. Wu, *Phys. Rev. Lett.*, 2020, **125**, 117203.
55 L. Gu and R. Wu, *Phys. Rev. B*, 2021, **103**, 014401.
56 P. C. Bunting, M. Atanasov, E. Damgaard-Møller, M. Perfetti, I. Crassee, M. Orlita, J. Overgaard, J. van Slageren, F. Neese and J. R. Long, *Science*, 2018, **362**, eaat7319.
57 V. Vieru, N. Iwahara and L. F. Chibotaru, *Sci. Rep.*, 2016, **6**, 24046.
58 G. T. Nguyen and L. Ungur, *Phys. Chem. Chem. Phys.*, 2021, **23**, 10303–10310.

59 G. T. Nguyen and L. Ungur, *Chem. – Eur. J.*, 2022, **28**, e202200227.
60 T. Shang, F. Lu, J. Tao and Y.-Q. Zhang, *J. Phys. Chem. A*, 2023, **127**, 3088–3095.
61 A. Mansikkamäki, A. A. Popov, Q. Deng, N. Iwahara and L. F. Chibotaru, *J. Chem. Phys.*, 2017, **147**, 124305.
62 Z. Zhu and J. Tang, *Chem. Soc. Rev.*, 2022, **51**, 9469–9481.
63 Y. Pang, N. Nöthling, M. Leutzsch, L. Kang, E. Bill, M. van Gastel, E. Reijerse, R. Goddard, L. Wagner, D. SantaLucia, S. DeBeer, F. Neese and J. Cornella, *Science*, 2023, **380**, 1043–1048.
64 C. Weetman and S. Inoue, *ChemCatChem*, 2018, **10**, 4213–4228.
65 J. D. Queen, A. Lehmann, J. C. Fettinger, H. M. Tuononen and P. P. Power, *J. Am. Chem. Soc.*, 2020, **142**, 20554–20559.
66 J. Hicks, P. Vasko, J. M. Goicoechea and S. Aldridge, *Angew. Chem., Int. Ed.*, 2021, **60**, 1702–1713.
67 M. P. Coles and M. J. Evans, *Chem. Commun.*, 2023, **59**, 503–519.
68 D. Wang, C. Zhai, Y. Chen, Y. He, X.-D. Chen, S. Wang, L. Zhao, G. Frenking, X. Wang and G. Tan, *Nat. Chem.*, 2023, **15**, 200–205.
69 D. Wang, W. Chen, H. Chen, Y. Chen, S. Ye and G. Tan, *Nat. Chem.*, 2025, **17**, 38–43.
70 S. H. F. Schreiner, T. Rüffer and R. Kretschmer, *Nat. Synth.*, 2025, **4**, 67–74.
71 M. He, C. Hu, R. Wei, X.-F. Wang and L. L. Liu, *Chem. Soc. Rev.*, 2024, **53**, 3896–3951.
72 A. Mansikkamäki, *Chem. Commun.*, 2023, **59**, 1837–1840.
73 F.-S. Guo, A. K. Bar and R. A. Layfield, *Chem. Rev.*, 2019, **119**, 8479–8505.
74 F.-S. Guo, M. He, G.-Z. Huang, S. R. Giblin, D. Billington, F. W. Heinemann, M.-L. Tong, A. Mansikkamäki and R. A. Layfield, *Inorg. Chem.*, 2022, **61**, 6017–6025.
75 P. Evans, D. Reta, G. F. S. Whitehead, N. F. Chilton and D. P. Mills, *J. Am. Chem. Soc.*, 2019, **141**, 19935–19940.
76 P. Zhang, F. Benner, N. F. Chilton and S. Demir, *Chem*, 2021, **8**, 717–730.
77 P. Zhang, R. Nabi, J. K. Staab, N. F. Chilton and S. Demir, *J. Am. Chem. Soc.*, 2023, **145**, 9152–9163.
78 F. Benner, E. R. Pugliese, R. Q. Marsden, R. J. Staples, N. F. Chilton and S. Demir, *Inorg. Chem.*, 2024, **63**, 20250–20256.
79 L. Pauling, *The Nature of the Chemical Bond*, Cornell University Press, Ithaca, NY, USA, 3rd edn, 1960.
80 H. A. Kramers, *Proc. K. Ned. Akad. Wet.*, 1930, **33**, 959–972.
81 E. Wigner, *Göttinger Nachr.*, 1932, **1932**, 546–559.
82 A. K. Zvezdin, B. M. Matveev, A. A. Mukhin and A. I. Popov, *Redkozemel'nyye Iony v Magnitouporyadochennykh Kristallakh*, Nauka, Moscow, Russia, 1985.
83 A. Abragam and B. Bleaney, *Electron Paramagnetic Resonance of Transition Ions*, Clarendon Press, Oxford, UK, 1970.
84 J. H. van Vleck, *Phys. Rev.*, 1940, **57**, 426–447.
85 R. Orbach, *Proc. R. Soc. A*, 1961, **264**, 458–484.
86 K. N. Shrivastava, *Phys. Status Solidi B*, 1983, **117**, 437–458.
87 L. Ungur and L. F. Chibotaru, *Phys. Chem. Chem. Phys.*, 2011, **13**, 20086–20090.
88 M. H. L. Pryce, *Proc. Phys. Soc., London, Sect. A*, 1950, **63**, 25.
89 J. S. Griffith, *Mol. Phys.*, 1960, **3**, 79–89.
90 L. F. Chibotaru, A. Ceulemans and H. Bolvin, *Phys. Rev. Lett.*, 2008, **101**, 033003.
91 L. F. Chibotaru, in *Advances in Chemical Physics*, ed. S. A. Rice and A. R. Dinner, Wiley, 2013, vol. 153, pp. 397–519.
92 S. Komorovsky, *arXiv*, 2023, preprint, arXiv:2305.06778, DOI: 10.48550/arXiv.2305.06778.
93 Y.-S. Ding, K.-X. Yu, D. Reta, F. Ortu, R. E. P. Winpenny, Y.-Z. Zheng and N. F. Chilton, *Nat. Commun.*, 2018, **9**, 3134.
94 A. Lunghi and S. Sanvito, *J. Chem. Phys.*, 2020, **153**, 174113.
95 J. S. Griffith, *The Theory of Transition-Metal Ions*, Cambridge University Press, Cambridge, UK, 1961.
96 C. J. Ballhausen, *Introduction to Ligand Field Theory*, McGraw-Hill, New York, NY, USA, 1962.
97 P. Pyykko, *Chem. Rev.*, 1988, **88**, 563–594.
98 K. G. Dyall and K. Fægri, Jr, *Introduction to Relativistic Quantum Chemistry*, Oxford University Press, Oxford, UK, 2007.
99 M. Reiher and A. Wolf, *Relativistic Quantum Chemistry*, Wiley-VCH, Weinheim, Germany, 2nd edn, 2015.
100 M. A. El-Sayed, *J. Chem. Phys.*, 1963, **38**, 2834–2838.
101 M. A. El-Sayed, *J. Chem. Phys.*, 1964, **41**, 2462–2467.
102 C. K. Jørgensen, *Structure And Bonding*, Springer, Berlin, Germany, 1966, vol. 1, pp. 3–31.
103 F. Neese and E. I. Solomon, *Inorg. Chem.*, 1998, **37**, 6568–6582.
104 H. A. Jahn and E. Teller, *Proc. R. Soc. A*, 1937, **161**, 220–235.
105 I. B. Bersuker, *The Jahn-Teller Effect*, Cambridge University Press, Cambridge, UK, 2006.
106 J. David, D. Guerra and A. Restrepo, *Inorg. Chem.*, 2011, **50**, 1480–1483.
107 T. Zeng, D. G. Fedorov, M. W. Schmidt and M. Klobukowski, *J. Chem. Theory Comput.*, 2011, **7**, 2864–2875.
108 P. P. Power, *Chem. Rev.*, 1999, **99**, 3463–3504.
109 R. C. Fischer and P. P. Power, *Chem. Rev.*, 2010, **110**, 3877–3923.
110 G. Herzberg, *Molecular Spectra and Molecular Structure. I. Spectra of Diatomic Molecules*, D. van Nostrand Company, New York, NY, USA, 2nd edn, 1950.
111 A. Szabo and N. S. Ostlund, *Modern Quantum Chemistry*, Macmillan Publishing Company, New York, NY, USA, 1982.
112 E. U. Condon and G. H. Shortley, *The Theory of Atomic Spectra*, Cambridge University Press, Cambridge, UK, 1935.
113 T. Helgaker, P. Jørgensen and J. Olsen, *Molecular Electronic-Structure Theory*, Wiley, Chichester, UK, 2000.
114 P. Jørgensen and J. Simons, *Second Quantization-Based Methods in Quantum Chemistry*, Academic Press, New York, NY, USA, 1981.
115 B. R. Judd, *Second Quantization and Atomic Spectroscopy*, The Johns Hopkins Press, Baltimore, MD, USA, 1967.
116 H. L. C. Feltham, Y. Lan, F. Klöwer, L. Ungur, L. F. Chibotaru, A. K. Powell and S. Brooker, *Chem. – Eur. J.*, 2011, **17**, 4362–4365.

117 F. Habib, J. Long, P.-H. Lin, I. Korobkov, L. Ungur, W. Wernsdorfer, L. F. Chibotaru and M. Murugesu, *Chem. Sci.*, 2012, **3**, 2158–2164.
118 C. Jin, X.-L. Li, Z. Liu, A. Mansikkamäki and J. Tang, *Dalton Trans.*, 2020, **49**, 10477–10485.
119 D. Errulat, K. L. M. Harriman, D. A. Gálico, A. A. Kitos, A. Mansikkamäki and M. Murugesu, *Nat. Chem.*, 2023, **15**, 1100–1107.
120 T. Shirai, J. Reader, A. E. Kramida and J. Sugar, *J. Phys. Chem. Ref. Data*, 2007, **36**, 509–615.
121 G. V. Deverall, K. W. Meissner and G. J. Zissis, *Phys. Rev.*, 1953, **91**, 297–299.
122 C. E. Moore, *Atomic Energy Levels as Derived from the Analysis of Optical Spectra – Molybdenum through Lanthanum and Hafnium through Actinium*, National Bureau of Standards, USA, 1971.
123 C. E. Housecroft and A. G. Sharpe, *Inorganic Chemistry*, Pearson Education Limited, Harlow, UK, 3rd edn, 2008.
124 N. N. Greenwood and A. Earnshaw, *Chemistry of the Elements*, Butterworth-Heineman, Oxford, UK, 2nd edn, 1997.
125 F. A. Cotton and G. Wilkinson, *Advanced Inorganic Chemistry*, Wiley, New York, NY, USA, 4th edn, 1980.
126 P. Atkins, T. Overton, J. Rourke, M. Weller and F. Armstrong, *Shiver & Atkins' Inorganic Chemistry*, Oxford University Press, Oxford, UK, 2nd edn, 2010.
127 R. E. Marsh and D. P. Shoemaker, *Acta Crystallogr.*, 1953, **6**, 197–205.
128 I. F. Hewaidy, E. Busmann and W. Klemm, *Z. Anorg. Allg. Chem.*, 1964, **328**, 283–293.
129 R. Thümmel and W. Klemm, *Z. Anorg. Allg. Chem.*, 1970, **376**, 44–63.
130 M. Abraham, Y. Wang, Y. Xie, P. Wei, H. Schaefer III, P. V. R. Schleyer and G. Robinson, *Chem. – Eur. J.*, 2010, **16**, 432–435.
131 L. P. Ho, A. Nasr, P. G. Jones, A. Altun, F. Neese, G. Bistoni and M. Tamm, *Chem. – Eur. J.*, 2018, **24**, 18922–18932.
132 L. P. Ho and M. Tamm, *Dalton Trans.*, 2021, **50**, 1202–1205.
133 A. Mardyukov, Y. A. Tsegaw, W. Sander and P. R. Schreiner, *Phys. Chem. Chem. Phys.*, 2017, **19**, 27384–27388.
134 F. Keul, A. Mardyukov and P. R. Schreiner, *Phys. Chem. Chem. Phys.*, 2019, **21**, 25797–25801.
135 N. Bobrowski, G. Hönninger, B. Galle and U. Platt, *Nature*, 2003, **423**, 273–276.
136 A. Saiz-Lopez, J. M. C. Plane, A. R. Baker, L. J. Carpenter, R. von Glasow, J. C. Gómez Martín, G. McFiggans and R. W. Saunders, *Chem. Rev.*, 2012, **112**, 1773–1804.
137 P. P. Power, *Chem. Rev.*, 2003, **103**, 789–810.
138 *Stable Radicals*, ed. R. G. Hicks, Wiley, Chichester, UK, 2010.
139 E. J. Baerends, T. Ziegler, A. J. Atkins, J. Autschbach, O. Baseggio, D. Bashford, A. Bérces, F. M. Bickelhaupt, C. Bo, P. M. Boerrigter, C. Cappelli, L. Cavallo, C. Daul, D. P. Chong, D. V. Chulhai, L. Deng, R. M. Dickson, J. M. Dieterich, F. Egidi, D. E. Ellis, M. van Faassen, L. Fan, T. H. Fischer, A. Förster, C. F. Guerra, M. Franchini, A. Ghysels, A. Giammona, S. J. A. van Gisbergen, A. Goez, A. W. Götz, J. A. Groeneveld, O. V. Gritsenko, M. Grüning, S. Gusarov, F. E. Harris, P. van den Hoek, Z. Hu, C. R. Jacob, H. Jacobsen, L. Jensen, L. Joubert, J. W. Kaminski, G. van Kessel, C. König, F. Kootstra, A. Kovalenko, M. V. Krykunov, P. Lafiosca, E. van Lenthe, D. A. McCormack, M. Medves, A. Michalak, M. Mitoraj, S. M. Morton, J. Neugebauer, V. P. Nicu, L. Noodleman, V. P. Osinga, S. Patchkovskii, M. Pavanello, C. A. Peeples, P. H. T. Philipsen, D. Post, C. C. Pye, H. Ramanantoanina, P. Ramos, W. Ravenek, M. Reimann, J. I. Rodríguez, P. Ros, R. Rüger, P. R. T. Schipper, D. Schlüns, H. van Schoot, G. Schreckenbach, J. S. Seldenthuis, M. Seth, J. G. Snijders, M. Solà, M. Stener, M. Swart, D. Swerhone, V. Tognetti, G. te Velde, P. Vernooijs, L. Versluis, L. Visscher, O. Visser, F. Wang, T. A. Wesolowski, E. M. van Wezenbeek, G. Wiesenekker, S. K. Wolff, T. K. Woo and A. L. Yakovlev, *ADF2023*, 2023, **https://www.scm.com**.
140 G. te Velde, F. M. Bickelhaupt, E. J. Baerends, C. Fonseca Guerra, S. J. A. van Gisbergen, J. G. Snijders and T. Ziegler, *J. Comput. Chem.*, 2001, **22**, 931–967.
141 R. Rüger, M. Franchini, T. Trnka, A. Yakovlev, E. van Lenthe, P. Philipsen, T. van Vuren, B. Klumpers and T. Soini, *AMS2023*, 2023, **https://www.scm.com**.
142 B. O. Roos, in *Advances in Chemical Physics: Ab Initio Methods in Quantum Chemistry II*, ed. K. P. Lawley, Wiley, New York, NY, USA, 1987, vol. 69, pp. 399–455.
143 B. O. Roos, R. Lindh, P. Å. Malmqvist, V. Veryazov and P.-O. Widmark, *Multiconfigurational Quantum Chemistry*, Wiley, Hoboken, NJ, USA, 2016.
144 C. Angeli, R. Cimiraglia, S. Evangelisti, T. Leininger and J.-P. Malrieu, *J. Chem. Phys.*, 2001, **114**, 10252–10264.
145 C. Angeli, R. Cimiraglia and J.-P. Malrieu, *Chem. Phys. Lett.*, 2001, **350**, 297–305.
146 C. Angeli, R. Cimiraglia and J.-P. Malrieu, *J. Chem. Phys.*, 2002, **117**, 9138–9153.
147 F. Neese, *Wiley Interdiscip. Rev.:Comput. Mol. Sci.*, 2017, **8**, e1327.
148 F. Neese, F. Wennmohs, U. Becker and C. Riplinger, *J. Chem. Phys.*, 2020, **152**, 224108.
149 F. Neese, *J. Comput. Chem.*, 2022, **44**, 381–396.
150 F. Neese, T. Petrenko, D. Ganyushin and G. Olbrich, *Coord. Chem. Rev.*, 2007, **251**, 288–327.
151 P. P. Power, *Organometallics*, 2020, **39**, 4127–4138.
152 P. Pyykko and J. P. Desclaux, *Acc. Chem. Res.*, 1979, **12**, 276–281.
153 T. Matsuo, K. Suzuki, T. Fukawa, B. Li, M. Ito, Y. Shoji, T. Otani, L. Li, M. Kobayashi, M. Hachiya, Y. Tahara, D. Hashizume, T. Fukunaga, A. Fukazawa, Y. Li, H. Tsuji and K. Tamao, *Bull. Chem. Soc. Jpn.*, 2011, **84**, 1178–1191.
154 C. Riplinger and F. Neese, *J. Chem. Phys.*, 2013, **138**, 034106.
155 C. Riplinger, B. Sandhoefer, A. Hansen and F. Neese, *J. Chem. Phys.*, 2013, **139**, 134101.
156 C. Riplinger, P. Pinski, U. Becker, E. F. Valeev and F. Neese, *J. Chem. Phys.*, 2016, **144**, 024109.
157 M. Saitow, U. Becker, C. Riplinger, E. F. Valeev and F. Neese, *J. Chem. Phys.*, 2017, **146**, 164105.

158 Y. Guo, C. Riplinger, U. Becker, D. G. Liakos, Y. Minenkov, L. Cavallo and F. Neese, *J. Chem. Phys.*, 2018, **148**, 011101.
159 A. V. Marenich, J. Ho, M. L. Coote, C. J. Cramer and D. G. Truhlar, *Phys. Chem. Chem. Phys.*, 2014, **16**, 15068–15106.
160 W.-J. Xu, Q.-C. Luo, Z.-H. Li, Y.-Q. Zhai and Y.-Z. Zheng, *Adv. Sci.*, 2024, **11**, 2308548.
161 J. Emerson-King, G. Gransbury, B. Atkinson, W. Blackmore, G. Whitehead, N. Chilton and D. Mills, *ChemRxiv*, 2024, preprint, DOI: **10.26434/chemrxiv-2024-36vjp**.
162 A. Bondi, *J. Phys. Chem.*, 1964, **68**, 441–451.
163 M. Mantina, A. C. Chamberlin, R. Valero, C. J. Cramer and D. G. Truhlar, *J. Phys. Chem. A*, 2009, **113**, 5806–5812.
164 P. Pyykkö and M. Atsumi, *Chem. – Eur. J.*, 2009, **15**, 186–197.
165 D. Errulat, K. L. M. Harriman, D. A. Gálico, E. V. Salerno, J. van Tol, A. Mansikkamäki, M. Rouzières, S. Hill, R. Clérac and M. Murugesu, *Nat. Commun.*, 2024, **15**, 3010.
166 J. Emerson-King, G. K. Gransbury, G. F. S. Whitehead, I. N. J. Vitorica-Yrezabal, M. Rouzières, R. Clérac, N. F. Chilton and D. P. Mills, *J. Am. Chem. Soc.*, 2024, **146**, 3331–3342.
167 L. Chibotaru, L. Ungur, N. Iwahara, W. Zhang and A. Muhtadi, *Angew. Chem., Int. Ed.*, 2020, **59**, 12720–12724.
168 K. L. Mears and P. P. Power, *Acc. Chem. Res.*, 2022, **55**, 1337–1348.
169 K. S. Pedersen, J. Dreiser, H. Weihe, R. Sibille, H. V. Johannesen, M. A. Sørensen, B. E. Nielsen, M. Sigrist, H. Mutka, S. Rols, J. Bendix and S. Piligkos, *Inorg. Chem.*, 2015, **54**, 7600–7606.

